catalysts

MDPI

Article

Green Synthesis of AuNPs by *Crocus caspius*—Investigation of Catalytic Degradation of Organic Pollutants, Their Cytotoxicity, and Antimicrobial Activity

Seyedeh Roya Alizadeh [1], Pourya Biparva [2], Hamid Reza Goli [1], Barkat Ali Khan [3] and Mohammad Ali Ebrahimzadeh [1,*]

[1] Department of Medicinal Chemistry, School of Pharmacy and Pharmaceutical Sciences Research Center, Mazandaran University of Medical Sciences, Sari 48471-93698, Iran
[2] Department of Basic Sciences, Sari University of Agricultural Sciences and Natural Resources, Sari 48181-68984, Iran
[3] Drug Delivery and Cosmetics Lab (DDCL), GCPS, Faculty of Pharmacy, Gomal University, Dera Ismail Khan 29050, Pakistan
* Correspondence: zadeh20@gmail.com

Abstract: Biogenic methods are an effective alternative to chemical methods in the preparation of nanoparticles. Our study used *Crocus caspius* extract to synthesize gold nanoparticles (CC-AuNPs) in a green manner. The eco-friendly synthesis of AuNPs was conducted by optimizing the temperature and concentration of $HAuCl_4$ and extract. Synthesized CC-AuNPs were characterized using TEM, SEM, EDX, XRD, FTIR, and UV–Vis spectroscopy. The prepared CC-AuNPs were detected with a size of around 22.66 ± 1.67 nm. The FT-IR analysis of the biomolecules involved in synthesizing CC-AuNPs was performed. Additionally, these biomolecules capped on the AuNPs were revealed by TG/DTA analysis. The EDX study demonstrated the existence of elemental gold. The biosynthesized CC-AuNPs were effectively applied as green catalysts to reduce three organic pollutant dyes—methyl orange (MO), methylene blue (MB), and 4-nitrophenol. In the biological evaluations, the free radical scavenging activity of the eco-friendly CC-AuNPs (DPPH assay) indicated an IC_{50} value of 29.22 ± 0.47 µg/mL. They displayed effective antibacterial activity against several bacterial strains. Their anticancer activity against AGS and MCF-7 cells showed IC_{50} concentrations at 48.2 µg/mL and 51.76 µg/mL, respectively. Furthermore, CC-AuNPs presented excellent antileishmanial activity (IC_{50} = 13.92 µg/mL). Therefore, the green AuNPs are efficient in biomedicine and nanobiotechnology.

Keywords: gold nanoparticles; *Crocus caspius*; anticancer; antibacterial; antileishmanial; catalytic effects

check for updates

Citation: Alizadeh, S.R.; Biparva, P.; Goli, H.R.; Khan, B.A.; Ebrahimzadeh, M.A. Green Synthesis of AuNPs by *Crocus caspius*—Investigation of Catalytic Degradation of Organic Pollutants, Their Cytotoxicity, and Antimicrobial Activity. *Catalysts* **2023**, *13*, 63. https://doi.org/10.3390/catal13010063

Academic Editors: Seshibe S. Makgato and Evans Martin Nkhalambayausi Chirwa

Received: 30 November 2022
Revised: 20 December 2022
Accepted: 23 December 2022
Published: 28 December 2022

Copyright: © 2022 by the authors. Licensee MDPI, Basel, Switzerland. This article is an open access article distributed under the terms and conditions of the Creative Commons Attribution (CC BY) license (https://creativecommons.org/licenses/by/4.0/).

1. Introduction

Along with the rapid growth in cancer patients in recent decades, research into the fields of treatment and prevention has constantly increased. As examples, one could mention breast cancer, which has been announced as the most frequent type in women worldwide [1], and pancreatic cancer, for which medical records have shown an increase in the death rate due to this disease. As an alternative to the current methods, i.e., chemotherapy, radiotherapy, or surgery, many research efforts have focused on the anticancer activity of biosynthesized nanoparticles to combat cancer [2,3]. The nanotechnology-based therapeutics, as an association between the fields of nanotechnology and biotechnology, have displayed promising opportunities for cancer therapy, antimicrobial, and catalytic applications [4,5].

Over the last few decades, nanotechnology has incontrovertibly influenced cutting-edge research on biomedical and cancerous therapy. The main concerning areas regarding the potential application of nanomaterials in biomedicine are tuning size, the surface-to-volume ratio, and structure [6], and approaching a cost-effective, environment-friendly,

and biocompatible synthesis protocol. Among the most-studied nanomaterials, gold nanoparticles (AuNPs), which are distinguished by their fascinating antibacterial features, oxidation resistance, and anti-inflammatory activities [7], have garnered unprecedented attention for this purpose [8].

Several limitations and disadvantages concerning chemical and physical approaches for synthesizing biocompatible AuNPs have derived the motivation toward developing eco-friendly and bio-inspired synthesis routes. Green chemistry has emerged as a well-known strategy to toggle over difficulties such as hazardous by-products because of its biocompatibility and more facile control of particle size. As an environmentally safe method, green synthesis using micro-organisms and plant extracts instead of chemical substances, uses a versatile route to reduce Au ions to functionalized nano-biological, well-defined Au nanoparticles [2,9,10]. In this regard, a double role, either reducing or stabilizing, has been speculated for the plant extracts [11]. In recent years, different kinds of plant extract have been used to prepare noble metal NPs. Some plants involved in AuNPs synthesis can be mentioned: *convolvulus fruticosus* [10], *crataegus monogyna* [9], *Lonicera japonica* flower [12], *Azadirachta indica* [13], *Stenotrophomonas maltophilia* [14], *Crocus sativus* [15,16], *barberry* [17], *Coffea arabica* seed [18], and *Stevia rebadiauna* leaf extracts [19]. However, despite all the recent endeavors that have been devoted to synthesizing AuNPs via bio-reductants, it is highly desirable to put forward an even more convenient and easy-to-perform procedure for better control of the size, shape, and surface functionalization of nanoparticles with antibacterial and anticancer activities.

The features mentioned above would render the biosynthesized AuNPs without deficiencies such as toxicity, which makes them favorable for cancer therapy [11]. In addition, it has been reported that the green synthesis method promotes the antimicrobial activity of metal nanoparticles. The size of the NPs is the crucial parameter in this regard [20]. Different mechanisms have been reported for the antimicrobial performance of AuNPs, such as electrostatic interaction between NPs and the cell membrane of micro-organisms, and the perforation of bacterial cell walls by AuNPs, which leads to cell death [21]. Furthermore, nanoparticles with smaller sizes and higher surface-to-volume ratios would more easily attach to the microbial membrane and subsequently penetrate it [22].

Another important property of gold nanoparticles is their catalytic effect, which stems from electronic charge distribution on their surfaces [18]. Moreover, by considering the electron transfer character, or the so-called electron relay effect, nanoparticles exert redox catalytic activity [7]. Recently, the successful catalytic performance of AuNPs in the degradation of Congo red and methyl orange has been reported [6]. Keeping this in mind, the catalytic activity of biosynthesized AuNPs is highly advantageous for reducing the environmental pollutants due to dye efflux from industries [10].

The present work deals with the green synthesis of AuNPs employing the extract of *Crocus caspius* as a reducing and capping agent. It has been proved that the extract of Caspian saffron, *Crocus caspius*, which is an endemic plant that grows in the south of the Caspian Sea, can be used as an antimicrobial agent [23,24]. Saffron is generally well-known for its antioxidant and antimicrobial properties, which have been applied in traditional Iranian folk medicines without any toxic side effects [24,25]. It is believed that its antioxidant property is due to the presence of phenolic compounds and carotenoids. These fascinating characteristics have been our motivation to prepare AuNPs mediated by the extract of *C. caspius* for the first time. The effects of different variables, such as AuNPs concentration, extract concentration, and reaction temperature, have also been studied in the green synthesis of AuNPs by *C. caspius* extract. Different characterization methods, including UV-Vis, SEM, TEM, EDX, DLS, zeta potential, and TG/DTA, were discussed to optimize the structural and physical properties. The anticancer activity of CC-AuNPs in vitro was examined by MTT assay against two cancer cell lines (MCF-7 and AGS). The antibacterial assessments were performed against several gram-positive and -negative strains of ATCC bacteria. Moreover, the radical scavenging (DPPH assay), antifungal, and antileishmanial activities of CC-AuNPs were investigated. Finally, the catalytic effects of

prepared CC-AuNPs were studied to reduce methylene blue (MB), methyl orange (MO), and 4-nitrophenol (4-NP) in the presence of $NaBH_4$ by UV–Vis spectroscopy.

2. Results and Discussion

2.1. Characterization of Synthesized CC-AuNPs

In this work, as the *C. caspius* extract was added to the chloroauric acid ($HAuCl_4 \cdot 3H_2O$) solution, the solution color slowly changed from yellow to ruby red after 30 min because of the reduction of Au (III) ions to Au(0), which shows the fabrication of AuNPs; thus, monitoring through UV–Vis spectroscopy is a useful technique. The formation of gold nanoparticles was represented by the broad surface plasmon resonance (SPR) peak around 570 nm (Figure 1). Various reaction conditions affected the UV–Vis spectra (Figure 1a–c) [26]. As shown in Figure 1a, to determine the optimum conditions, the concentrations of 6.348, 5.078, 3.809, 2.539, and 1.269 mM from $HAuCl_4 \cdot 3H_2O$ in deionized water were mixed with CC-extract (100 mg/10 mL) at 80 °C and 400 rpm, indicating the peak absorption increased concentration-dependent manner. Increasing the concentration of the gold salt resulted in negligible differences in the λ_{max} position. Therefore, 5.078 mM of $HAuCl_4 \cdot 3H_2O$ was considered to be the optimum concentration for gold salt. Temperature is another essential parameter that affects the production of gold nanoparticles; the optimization of the temperature factor in the green synthesis of AuNPs was represented at the UV–Vis spectra in Figure 1b; 3.809 mM of $HAuCl_4 \cdot 3H_2O$ was mixed with CC-extract (100 mg/10 mL) at 40, 60, 80, and 90 °C, resulting higher peak absorbance at 80 °C. Indeed, it can be seen that the SPR bands were found at almost at the same λ_{max} at higher temperatures, and the position of the peaks did not change noticeably. As shown in Figure 1c, various concentrations of *C. caspius* (25, 50, and 100 mg) were investigated to obtain the optimum concentration in the synthesis of CC-AuNPs; the best peak area was obtained for 100 mg CC-extract. Based on the results, the best conditions for the synthesis of gold nanoparticles observed were 5.078 mM Au salt and 100 mg CC-extract at 80 °C, which had the highest absorption peak at the wavelength of 570 nm compared to the others. The biosynthesis of AuNPs using *Ginkgo biloba* leaves was performed at the optimal conditions of 0.5 mM of $HAuCl_4$ solution, 0.5 mL of *G. biloba* extract, pH 10.0 at 60 °C for 30 min, yielding good stability, small sizes, and uniform distribution at SPR bands around 530 nm [27]. The green synthesis of AuNPs using the leaves extract of Commiphora wightii was proved by the change in the solution color from pale yellow to purple wine and the SPR bands at 533 nm [28]. In another study, AuNPs mediated by Pongamia pinnata leaves extract yielded absorption spectra with SPR bands in the 520–540 nm range [29].

TEM measurements have been employed to determine various the shapes and sizes of metal NPs. Therefore, in this work, CC-AuNPs were analyzed by TEM (Figure 2a), which displayed irregular shapes such as spherical, hexagonal, trigonal, and rods, but dominantly spherical or semi-spherical shapes with an average size of around 22.66 ± 1.67 nm for CC-AuNPs. In addition, the histogram obtained from the TEM image showed a size range of 8–45 nm for the prepared nanoparticles, which was consistent with the SEM histogram. The AuNPs produced by *Ginkgo biloba* leaves were well-dispersed and had various shapes, but were mainly spherical in nature [27]. The average size of AuNPs synthesized by Pongamia pinnata leaves extract was obtained in the range of 10–25 nm [29]. As shown in Figure 2b,c, the FE-SEM images present the surface morphology of *C. caspius*-prepared AuNPs at 500 nm and 1 µm magnifications. The micrograph at 1 µm magnification (Figure 2c) indicated a beautiful and irregular picture of the placement of synthesized nanoparticles in the residues of plant extract. In fact, FE-SEM images showed that the prepared AuNPs are embedded in the biomatrix. They are in a variety of shapes with an average particle size of about 30.98 ± 1.12 nm, which was close to the size calculated by the XRD analysis. Based on the histogram obtained from the SEM image, about 80% of synthesized nanoparticles were at 10–40 nm in size. The SEM micrograph of AuNPs capped with *Croton Caudatus Geisel* leaf extract revealed both individual AuNPs and a variety of aggregates. The TEM investigation revealed the produced AuNPs with spherical shapes and sizes of 20–50 nm [8].

SEM micrographs of *Sphaeranthus indicus*-prepared AuNPs indicated spherical morphology, and their TEM analysis displayed spherical shapes with an average size of 25 nm [30].

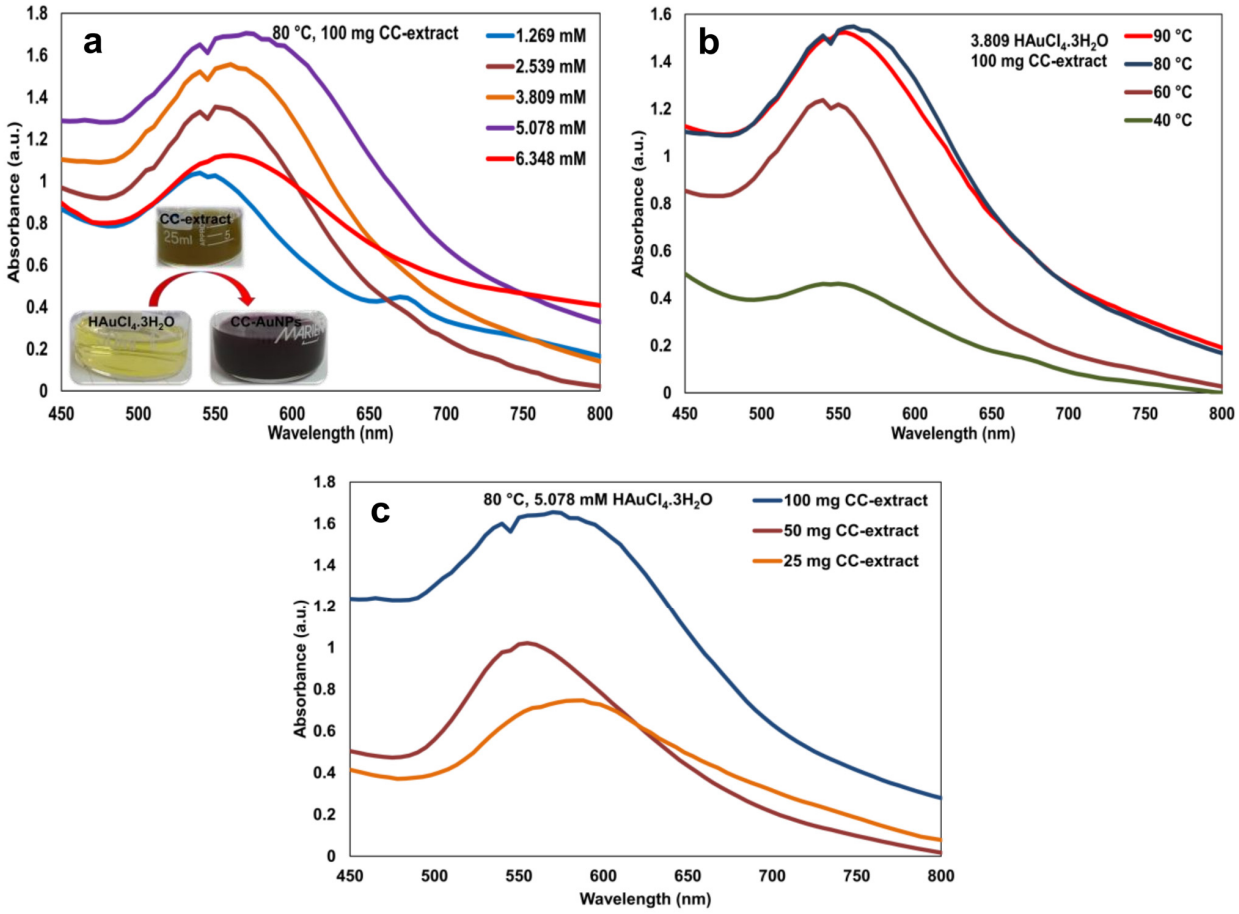


Figure 1. UV–Vis absorption spectra of CC-AuNPs: (**a**) various concentrations of $HAuCl_4 \cdot 3H_2O$ (6.348 mM, 5.078 mM, 3.809 mM, 2.539 mM, and 1.269 mM), (**b**) various temperatures (40, 60, 80, and 90 °C), and (**c**) various CC-extract concentrations (25, 50, and 100 mg).

EDX analysis was used to identify atomic compositions of CC-AuNPs, indicating a strong gold signal (2.2 keV) in the biosynthesized CC-AuNPs (Figure 3). In addition, the presence of C (0.27 keV), O (0.52 keV), and other impurities in the EDX spectra confirmed phytochemicals existing in the CC-extract [7,31,32]. The findings of Liu et al. proved the formation of AuNPs (by Zooglea ramigera) with EDX signals at 2.2 keV and 8.5 keV, which was similar to our result [33].

The hydrodynamic diameter of synthesized CC-AuNPs was assessed using DLS analysis, indicating the mean size of 101.4 ± 19.6 nm by number (Figure 4a,b). DLS analysis for gold nanoparticles synthesized by *Moringa oleifera* petals displayed an average hydrodynamic size of 203 nm [34]. In another study, the DLS analysis of AuNPs prepared using *Scutellaria barbata* yielded an average size of 154 nm [2]. It is to be expected that the particle size determined by TEM and DLS scattering differs slightly due to the differing measurement methods [34]. The stability of nanoparticles was determined by zeta potential that was determined as −30.8 ± 1.5 mV for the prepared CC-AuNPs. The phytochemicals, acting as capping agents, can produce repulsive forces on the surface of nanoparticles that make them stable [35].

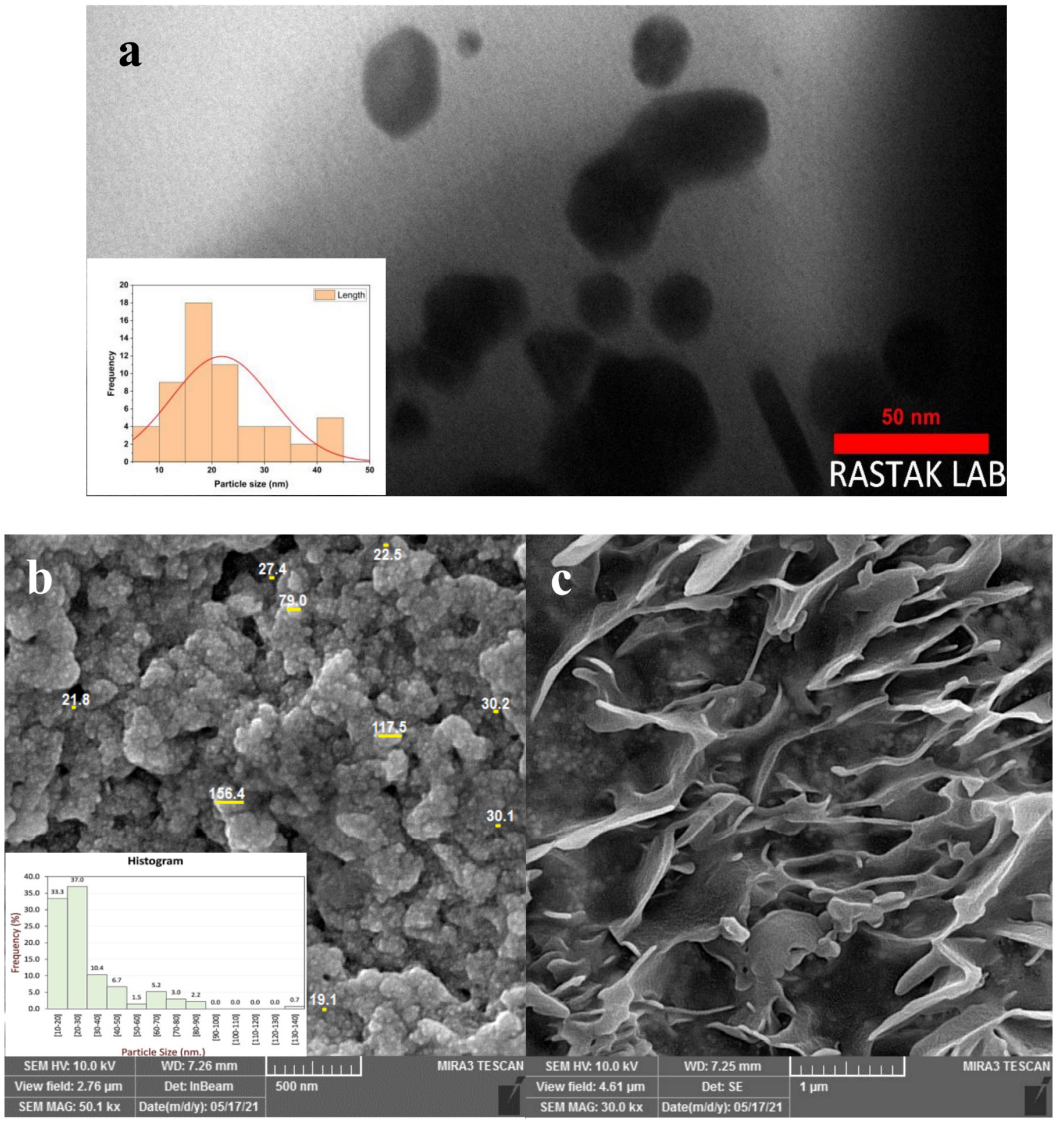


Figure 2. (**a**) The TEM image and the histogram reported from TEM image; (**b**,**c**) the SEM images at 500 nm and 1 µm magnifications and the histogram obtained from image 500 nm magnification.

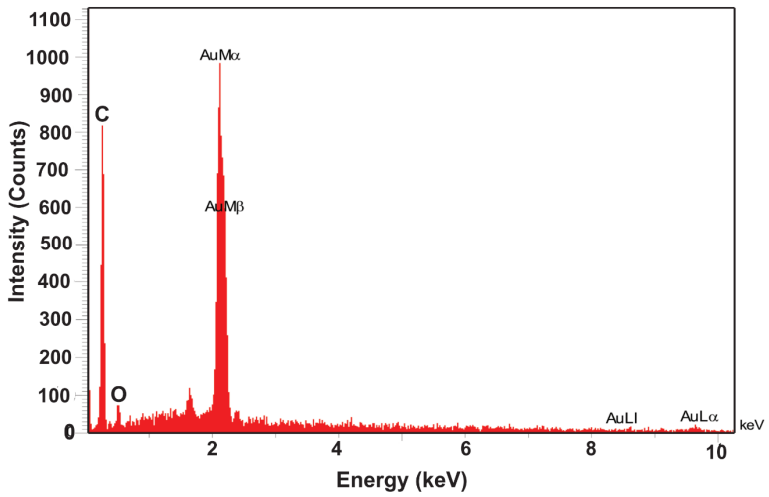


Figure 3. The EDX analysis of CC-AuNPs synthesized by *C. caspius* extract.

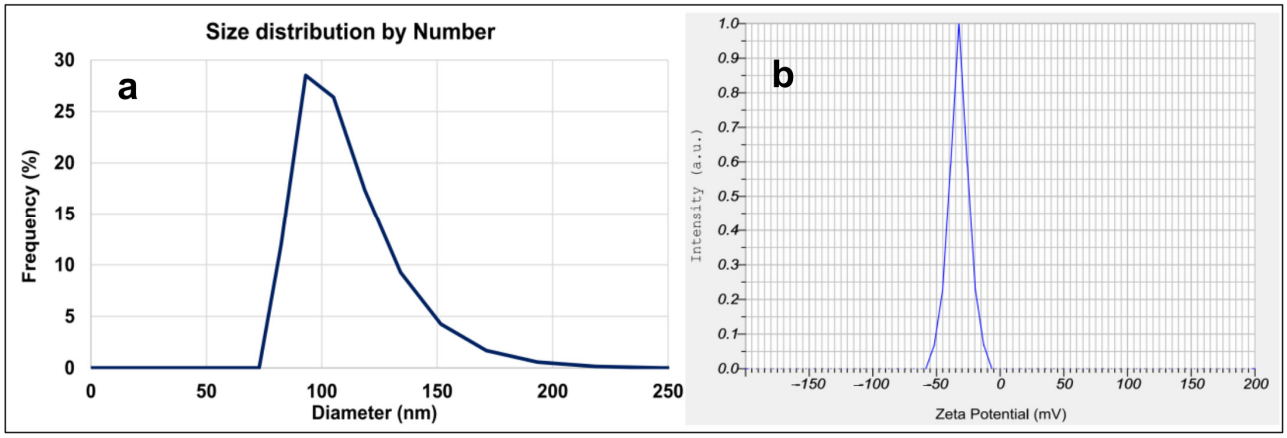


Figure 4. (**a**) Hydrodynamic particle size of CC-AuNPs using DLS (number-weighted) analysis (101.4 ± 19.6 nm), (**b**) zeta potential analysis of CC-AuNPs (−30.8 ± 1.5).

The FT-IR analysis was carried out to demonstrate the presence of the functional group and biomolecules in *C. caspius* extract. The roles of the extract as a reducer and a stabilizer stem from the availability of these groups. The FT-IR spectrum of the CC-extract and extract-mediated AuNPs (CC-AuNPs) is depicted in Figure 5. The peaks at 3285 cm^{-1} confirm the presence of the stretching vibration of phenolic hydroxyl [35,36]. The role of phenols as free radical scavengers has been clarified in recent years [23]. The peaks located at 2924 and 2854 cm^{-1} are associated with saturated hydrocarbons (Csp^3–H) [37]. Recently, it has been mentioned that the appearance of hydroxyl and carboxyl ions attests to the fact that the biomolecule could form the protective layers to stabilize the metal NPs [38]. The peak region of 2112 cm^{-1} was associated with stretching bands of the -C≡C- [4], 1624 cm^{-1} peak (stretching band of the carboxyl coupled to the amide I band) [39], 1708 cm^{-1} for carbonyl functional group [35], and C-N stretching vibrations of aliphatic amines and C-O stretching vibrations of alcohols at 1040 cm^{-1} have also been observed in our analysis [36,40]. The bands appearing at the wavenumbers 988 and 922 cm^{-1} indicate ν(=CH *trans* out of plane bending) and ν(=CH *cis* out of plane bending) vibrations [41,42]. As observed from the FT-IR spectra of the CC-AuNPs, the IR bands of the phenolic hydroxyl (around 3285 cm^{-1} in the case of the CC-extract) almost drastically vanished, which confirms their complete incorporation in the reduction and stabilization of the nanoparticles. In other words, through the breaking of O–H bonds and subsequent release of electrons due to the flavonoid and phenolic compounds, the Au (III) ions are converted into Au(0) [43]. Furthermore, this mechanism is speculated to be responsible for hindering the agglomeration of nanoparticles, which eventually control their size and shape [6]. Comparing the peak position of AuNPs with those of CC-extract, the peak intensity at 1694 cm^{-1} and 1590 cm^{-1} for CC-AuNPs diminished with slight shifts to lower wavenumber. After the production of CC-AuNPs, a sharp peak appeared at 2110 cm^{-1}, which related to the interaction between gold and CO. In other words, CO can be adsorbed on AuNPs and form CO-Au(0) species. In fact, this could be the reason for the decrease in the intensity of the peaks at 1694 and 1590 cm^{-1} in the AuNPs spectra [44]. Furthermore, one could distinguish some shifts to lower wavenumber, suggesting that the biomolecules act as capping agents on the surface of nanoparticles [1]. Our observations have clarified that phytochemical compounds (phenols, flavonoids) in the extract promote the formation of AuNPs and the binding of the biofunctional groups on the surface of synthesized AuNPs; these results are confirmed using several studies [32,34,45].

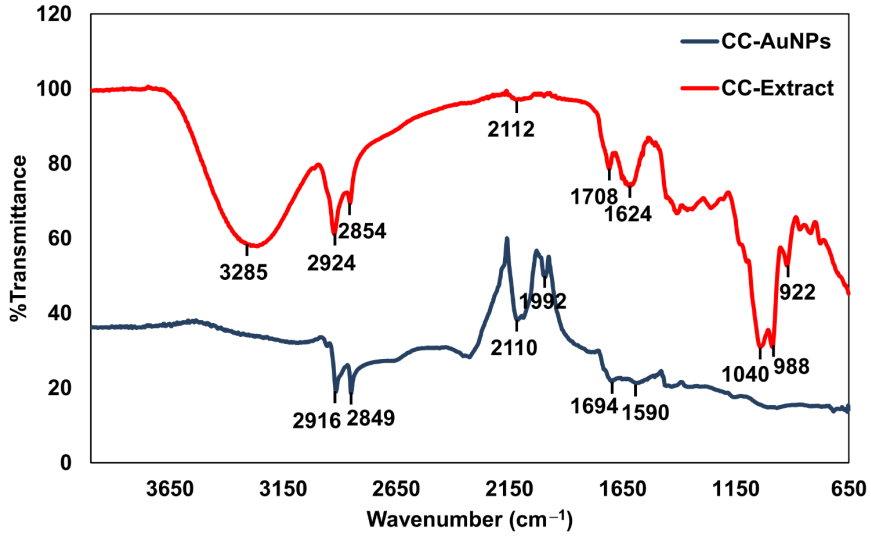


Figure 5. The FT-IR spectra for the *C. caspius* plant extract and biosynthesized AuNPs.

The crystalline nature of the NPs was evaluated by X-ray diffraction (XRD). The XRD pattern of biosynthesized AuNPs using the *C. caspius* extract is presented in Figure 6. The diffractogram shows four main diffraction peaks at about 2θ = 38°, 45°, 65°, and 78°, which are indexed to the (111), (200), (220), and (311) lattice planes, respectively. The identified peaks follow the reference of face-centered cubes (FCC) structure of metallic Au, from the Joint Committee of Powder Diffraction Standard (JCPDS) Card No-004–0784 [31,36]. The mean crystallite size of *C. caspius* extract-mediated AuNPs was found to be around 34.18 nm, which was calculated using the Debye–Scherrer equation (particle size $D = (k \times \lambda)/(\beta \cos\theta)$) [46]. The XRD studies of AuNPs prepared by a cheap *Sphaeranthus indicus* extract illustrated the FCC structure of metallic Au with a mean size of 37.96 nm [30].

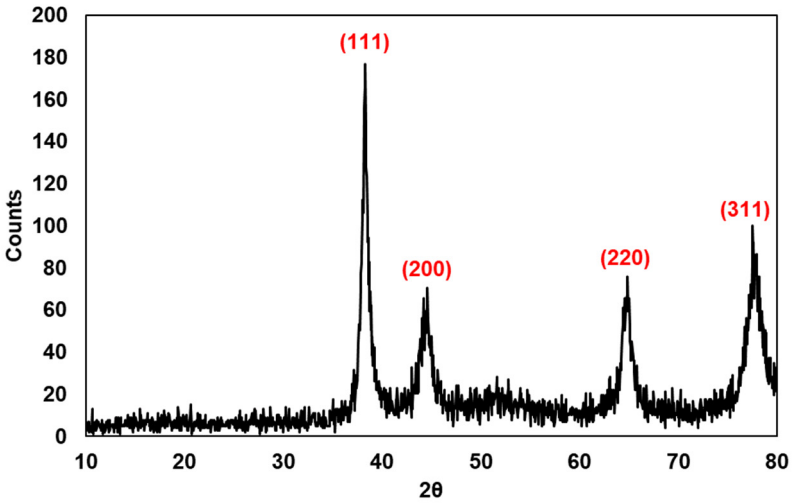


Figure 6. The XRD spectrum of biosynthesized CC-AuNPs.

TG/DTA analysis was applied to define the thermal stability and the total amount of phytochemical residuals of the synthesized CC-AuNPs [47]. The green synthesized CC-AuNPs were heated from 55 °C to 800 °C, indicating about 22% weight loss (Figure 7). Based on the TGA spectrum, weight loss was shown to occur in the ranges from 55 °C to 255 °C (with slight weight loss) and 255 °C to 455 °C (with high weight loss). The weight loss at 55 °C to 100 °C can be related to residual water evaporation [48]. In addition, the residual mass was related to the decomposition of capping biomolecules on the surface

of CC-AuNPs [48,49]. Higher temperatures showed no critical weight loss, indicating the thermal stability of CC-AuNPs.

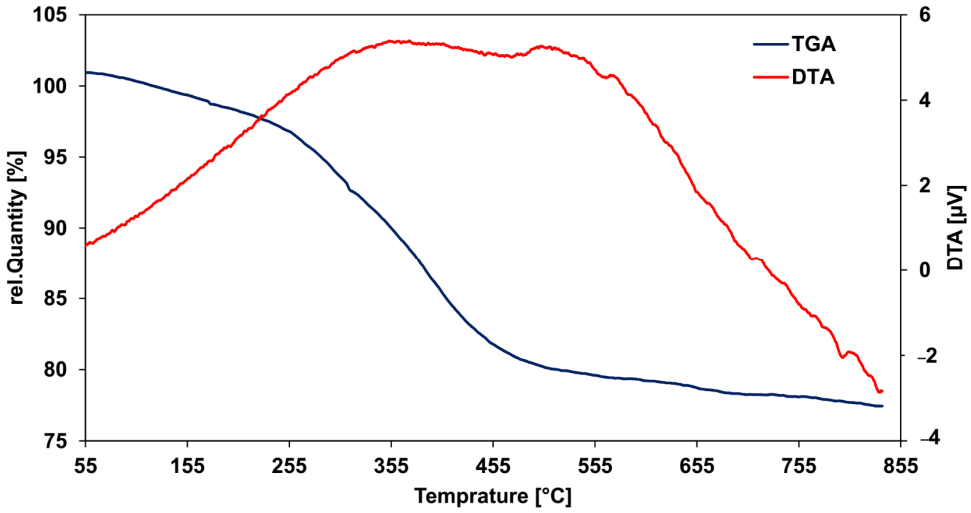


Figure 7. The TG/DTA pattern of biosynthesized CC-AuNPs.

2.2. HPLC Analysis

The HPLC method used for determining the content of flavonoids and phenolic acids in *C. caspius* extract used a binary isocratic solvent system. The HPLC analysis showed that the main bioactive compounds in this extract are gallic acid, catechin, caffeic acid, p-coumaric acid, and rutin (Table 1). HPLC analyses revealed that catechin was the major phenolic component in the extract with 8.4 mg/g plant, which was higher than other standards. The mechanism of AuNPs formation by phytochemicals existing in *C. caspius* extract is offered in Figure 8. The catechol moiety of the flavonoid structure or phenolic acids helps synthesize AuNPs; two e− are released from the ring, reducing Au(III) ions to Au(0), leading to the oxidation of catechol to 3′,4′-quinone ring. In the following, Au is aggregated to larger clusters and produces AuNPs. Furthermore, the quinone type of the bioactive compound is bound to the surface of NPs, reducing the aggregation of Au(0) on the nanoscale [50–53].

Table 1. The content of some phenolic acids in the extract of *C. caspius*.

Phenolic Acid	Retention Time (min)	*C. caspius* (mg/g)
Catechin	2.48	8.403
Gallic acid	3.58	0.14
p-Coumaric acid	9.76	0.107
Caffeic acid	17.28	0.027
Rutin	26.2	1.7

2.3. Antibacterial Activities of CC-AuNPs (MIC and MBC)

Minimum inhibitory concentration and minimum bactericidal concentration of CC-AuNPs were measured to evaluate their antibacterial activity against various bacterial strains Table 2. The MIC and MBC values of synthesized gold nanoparticles against several microorganisms were expressed in Table 2. The results showed that CC-AuNPs exhibited more activity against *S. aureus* and *K. pneumoniae* (MIC = 53.125 µg/mL), followed by *P. aeruginosa*, *A. baumannii*, *E. coli*, and *P. mirabilis* (MIC = 106.25 µg/mL), and *E. faecalis* (MIC = 212.5 µg/mL). Various studies have described the antimicrobial effect of AuNPs against different pathogens [47,49,54,55]. However, the action mechanism of NPs is not yet clarified in the inhibition of bacterial growth. Few studies have presented some hypotheses; the AuNPs can penetrate the organism's cell wall or cell membrane and interfere with their functions [31].

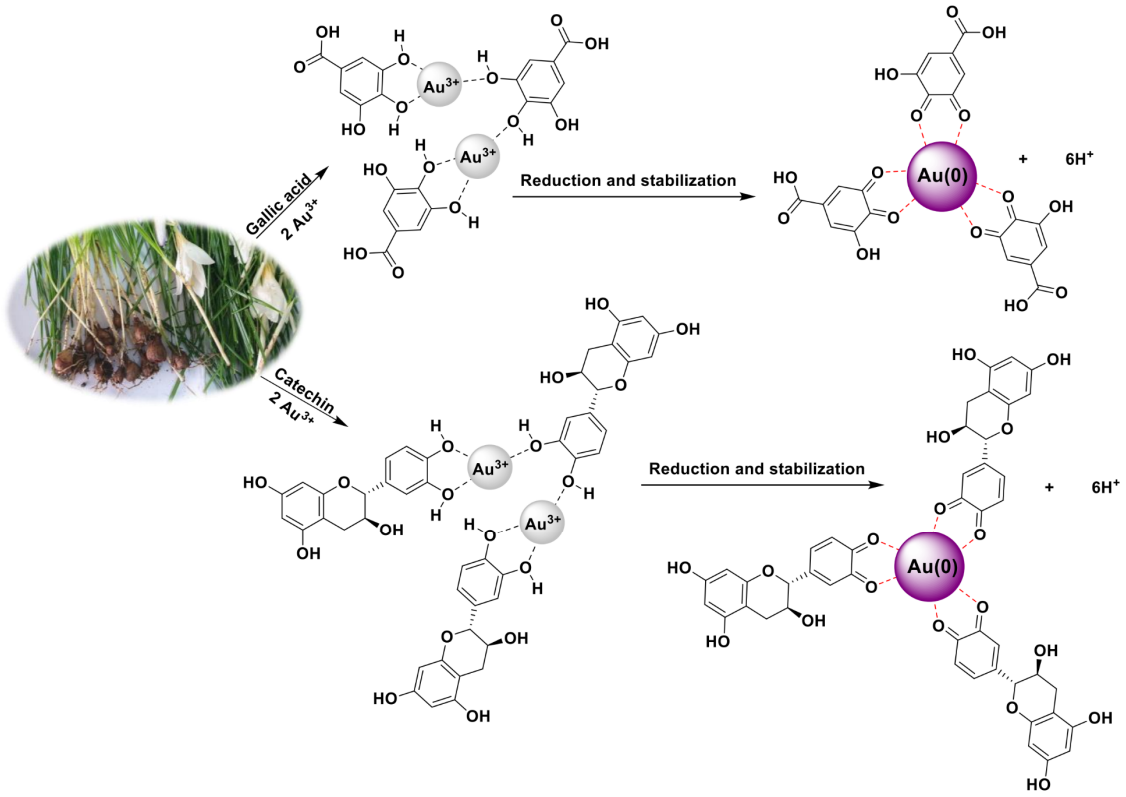


Figure 8. The probable mechanism of the green synthesis of AuNPs using C. caspius extract.

Table 2. The MIC and MBC values of CC-AuNPs against several gram-positive and gram-negative bacterial strains.

Bacteria	ATCC	CC-AuNPs		Extract	Ciprofloxacin
		MIC (μg/mL)	MBC (μg/mL)	MIC (μg/mL)	MIC (μg/mL)
S. aureus	ATCC 29213	53.125	850	>4000	0.21
E. faecalis	ATCC 29212	212.5	3400	>4000	0.21
P. aeruginosa	ATCC 27853	106.25	1700	>4000	0.3
A. baumannii	ATCC 19606	106.25	850	>4000	0.25
E. coli	ATCC 25922	106.25	1700	>4000	0.1
K. pneumoniae	ATCC 700603	53.125	850	>4000	0.1
P. mirabilis	ATCC 25933	106.25	850	>4000	0.1

2.4. Antileishmanial Activity

The treatment of leishmaniasis requires much attention because current treatment strategies are inefficient, expensive, and have severe toxic side effects; therefore, these problems complicate the control and treatment of the disease [56]. In this study, synthesized CC-AuNPs by *C. caspius* were examined against the in vitro antileishmanial activity. From the results, CC-AuNPs (212.5–6.64 μg/mL) displayed an IC_{50} value of 13.92 μg/mL, which was lower than that of amphotericin B (28.7 ± 2 μg/mL), the positive control. Therefore, the CC-AuNPs can be effective for leishmaniasis. Ahmad and coworkers showed antileishmanial activity of AuNPs synthesized by Sargentodoxa cuneata with an IC_{50} value of 5.29 μg/mL [57]. Besides, *Maytenus Royleanus*-mediated AuNPs presented 75% inhibition against the parasite growth [58]. According to the authors, the increased antileishmanial activity of AuNPs was due to a synergy between the surface-capped biomolecules and the antimicrobial properties of Au [56].

2.5. In Vitro Assay for Cytotoxicity Activity (MTT Assay)

The effect of synthesized NPs on cell viability was determined. Different concentrations of CC-AuNPs (1, 10, 25, 50, and 100 µg/mL) were tested by MTT assay for their cytotoxic effects on AGS, MCF-7, and HEK cells (Figure 9). These results determined that the green-synthesized CC-AuNPs had significant anticancer activities against AGS and MCF-7 cancer cell lines with the IC_{50} concentrations of 48.2 µg/mL and 51.76 µg/mL, respectively. Figure 9 shows the different cell viability percentages with varying concentrations of CC-AuNPs; as the concentration of CC-AuNPs was increased, cell growth reduced. The synthesized AuNPs inhibited the growth of AGS and MCF-7 cells by 24% and 29% at 1 µg/mL (the lowest tested concentration). The reference anticancer drug fluorouracil (5-FU) presented the IC_{50} concentrations of 44.25, 62.73, and 37.39 µg/mL in AGS, MCF-7, and HEK cells. Therefore, CC-AuNPs demonstrated anticancer activity close to 5-FU against two cancer cell lines, AGS and MCF-7. Uzma et al. showed that AuNPs prepared using *Commiphora wightii* had cytotoxic effects on MCF-7 cells with an IC_{50} of 66.11 µg/mL [28]. The cytotoxic effect of AuNPs with an extract of the red seaweed Corallina offcinalis was assessed in the MCF-7 cell line, and the concentration of biosynthesized AuNPs required to kill 50% of tumor cells was 1.5 µL/mL [59]. The green synthesized AuNPs displayed 81.9% cell inhibition against MCF-7 cells at the concentration of 2 µg/mL [60]. The cytotoxic mechanism may be due to free radicals production (ROS) from the green AuNPs [32].

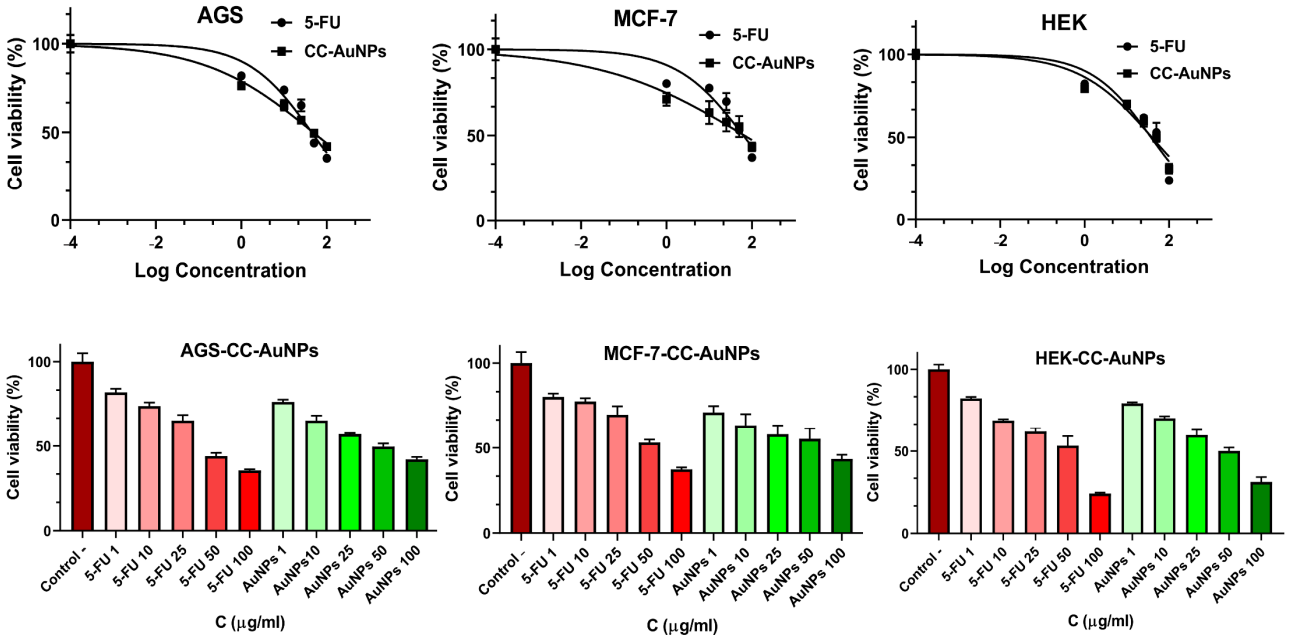


Figure 9. Cytotoxic effects of the prepared CC-AuNPs against MCF-7 and AGS cells and normal HEK cells during the treatment time of 24 h presented on two kinds of graph: log concentration vs cell viability %, and concentration vs cell viability %.

2.6. Antifungal Activity

The broth microdilution assay was applied to investigate the antifungal effect of CC-AuNPs against several resistant fungi strains. CC-AuNPs inhibited the growth of *Aspergillus* (1649), *Aspergillus* (1505), and *Trichophyton mentagrophytes* (FR1_22130) (Table 3) with an MIC value of 212.5 µg/mL; they did not exhibit activity against other tested strains. Hydrothermal green-prepared AuNPs using the mushroom extract (*A. bisporus*) exhibited a strong antifungal effect against *A. flavus* compared to *A. terreus* [61]. Furthermore, studies on the inhibitory mechanism suggested that gold ions cause loss of DNA, its ability to replicate, ribosomal subunit protein expression, and the expression of other cellular proteins and enzymes required for ATP generation on microorganisms, leading to the inactivation of living cells [62].

Table 3. The MIC value achieved from biosynthesized CC-AuNPs against fungi strains.

Fungi	CC-AuNPs	Extract	Itraconazole
	MIC (μg/mL)	MIC (μg/mL)	MIC (μg/mL)
Aspergillus fumigatus (IFRC1649)	212.5	>2500	≥16
Aspergillus fumigatus (IFRC1505)	212.5	>2500	≥16
Trichophyton mentagrophytes (FR1_22130)	212.5	>2500	≥16
Trichophyton mentagrophytes (FR5_22130)	R	>2500	16≥
Fusarium proliferatum (IFRC1871)	R	>2500	≥16
Fusarium equiseti (IFRC1872)	R	>2500	≥16
Candida albicans (IFRC1873)	R	>2500	≥16
Candida albicans (IFRC1874)	R	>2500	16≥

R; Resistant.

2.7. DPPH Assay

DPPH, a stable free radical, reacts with antioxidants, contributing H and causing reduction. The reaction color changes from red to yellow and can be recorded at the absorbance of 517 nm by UV–Vis spectrophotometry. Gold nanoparticles can donate e−or H- to DPPH free radicals and neutralize free radicals [22]. Due to the high surface area to volume ratio of AuNPs, they have a high affinity for the interaction with DPPH and its reduction [63]. Biosynthesized AuNPs have been offered as potent antioxidants in various studies [64–66]. In this work, the IC_{50} value of CC-AuNPs obtained was 29.22 ± 0.47 μg/mL. Butylated hydroxyanisole (BHA), a positive control, has an IC_{50} value of 53.96 μg/mL. Thus, the effect of free radical inhibition of synthesized CC-AuNPs was more effective than BHA.

2.8. Catalytic Activity on Degradation of Organic Dyes (MO, MB, and 4-NP)

One of the most challenging problems for the environment is the removal of non-biodegradable organic chemicals from industrial waste. Nanoparticles exert a potent degrading activity on organic dyes because of their high surface area [67]. In this work, the catalytic degradation of MO, MB, and 4-NP was studied in the presence of the prepared CC-AuNPs and NaBH4 (Figures 10–12). Various contents of CC-AuNPs (100, 120, and 150 μL × 425 μg/mL) were mixed with MO and $NaBH_4$ solution, changing the solution color (from orange to colorless) at 91, 46, and 21 min, respectively (Figure 10a–c). Based on the obtained data, a higher content of CC-AuNPs decreased the degradation reaction time (Figure 10d). As shown in Figure 10e, the absorbance spectrum of MO was unchanged without CC-AuNPs at 470 nm, even over 24 h. Therefore, the reduction reaction was very slow in the absence of a nanocatalyst. The reaction kinetics were pseudo-first order, and the MO degradation rate constants were calculated as 0.0219 min^{-1}, 0.04 min^{-1}, and 0.0729 min^{-1} for 100, 120, and 150 μL, respectively (Figure 10f). These data showed that the surface area of nanoparticles increased with increasing nanocatalyst content, therefore causing at increase in the reaction rate constant. The degradation percentages of MO using 100, 120, and 150 μL of the biofabricated CC-AuNPs were found to be 99, 99.3, and 100%, respectively (Figure 10g), showing the good catalytic effect of our AuNPs. The obtained results have been supported by previously published findings for green-prepared AuNPs as catalysts [26,68].

The degradation of MB solution by CC-AuNPs (150, 170, and 200 μL) with NaBH4 at 665 nm showed the solution color change from blue to colorless at 17, 15, and 13 min (Figure 11a–c). Figure 11d presents the comparison of degradation times at three nanocatalyst contents; the higher content of CC-AuNPs degraded MB in a shorter time. No MB degradation was detected in the presence of $NaBH_4$ only (Figure 11e). For the pseudo-first-order rate of the MB degradation reaction, the rate constants calculated were 0.1123, 0.1233, 0.1366 min^{-1} for 150, 170, and 200 μL of CC-AuNPs, respectively (Figure 11f). Therefore, adding catalytic amounts of CC-AuNPs to the dye solution containing $NaBH_4$ promoted the rate of the dye reduction reaction [26]. The degradation percentages of MB by 150, 170, and 200 μL of the synthesized CC-AuNPs obtained were 98, 98.6, and 99.5%, respectively

(Figure 11g), showing the good catalytic activity of AuNPs. Some reports were consistent with our findings [69–71].

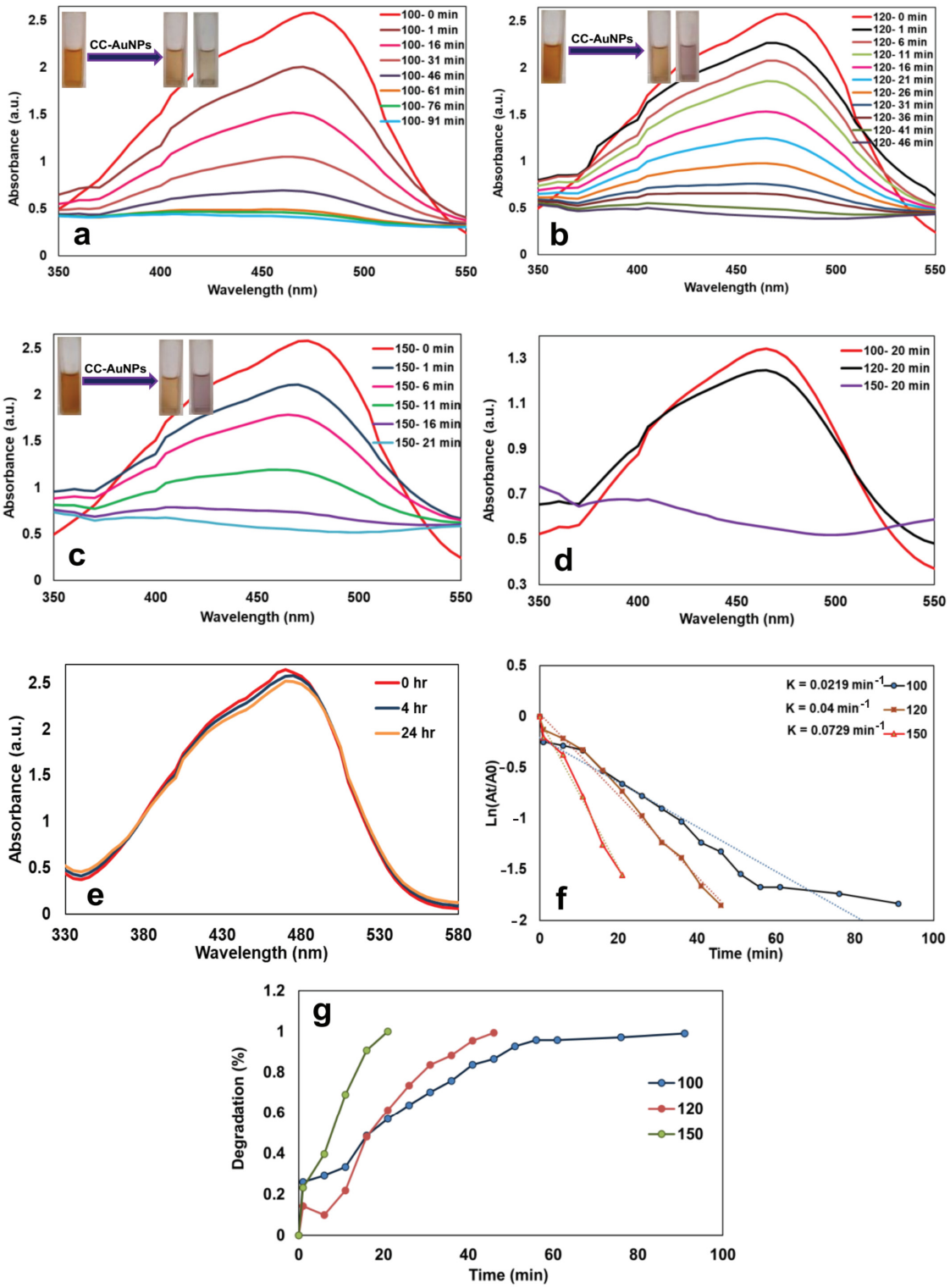


Figure 10. UV–Vis absorption spectra for the reduction of MO with $NaBH_4$ catalyzed by (**a**) 100 µL, (**b**) 120 µL, and (**c**) 150 µL of CC-AuNPs at the concentration 425 µg/mL, (**d**) the comparison of different volumes of CC-AuNPs. (**e**) UV–Vis spectra for the reduction of MO with $NaBH_4$ only without nanocatalyst; (**f**) the corresponding plots of ln(At/A0) vs. time, (**g**) degradation percentage of MO.

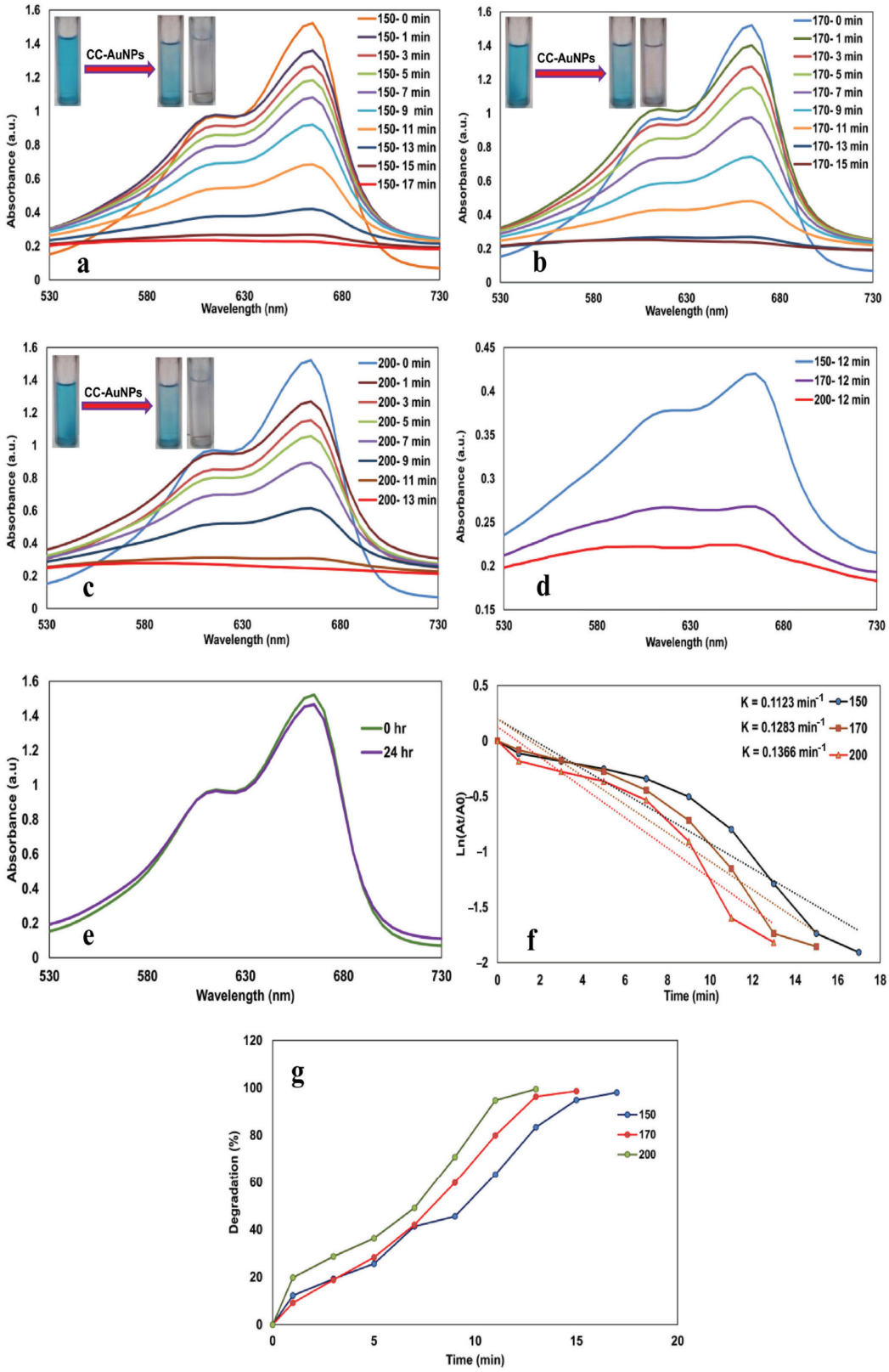


Figure 11. UV–Vis absorption spectra for the MB reduction with $NaBH_4$ catalyzed by (**a**) 150 µL, (**b**) 170 µL, and (**c**) 200 µL of CC-AuNPs (425 µg/mL), (**d**) the comparison of different volumes of CC-AuNPs. (**e**) UV–Vis spectra for the MB reduction with $NaBH_4$ only, without nanocatalyst, (**f**) the corresponding plots of ln(At/A0) vs time, (**g**) degradation percentage of MB.

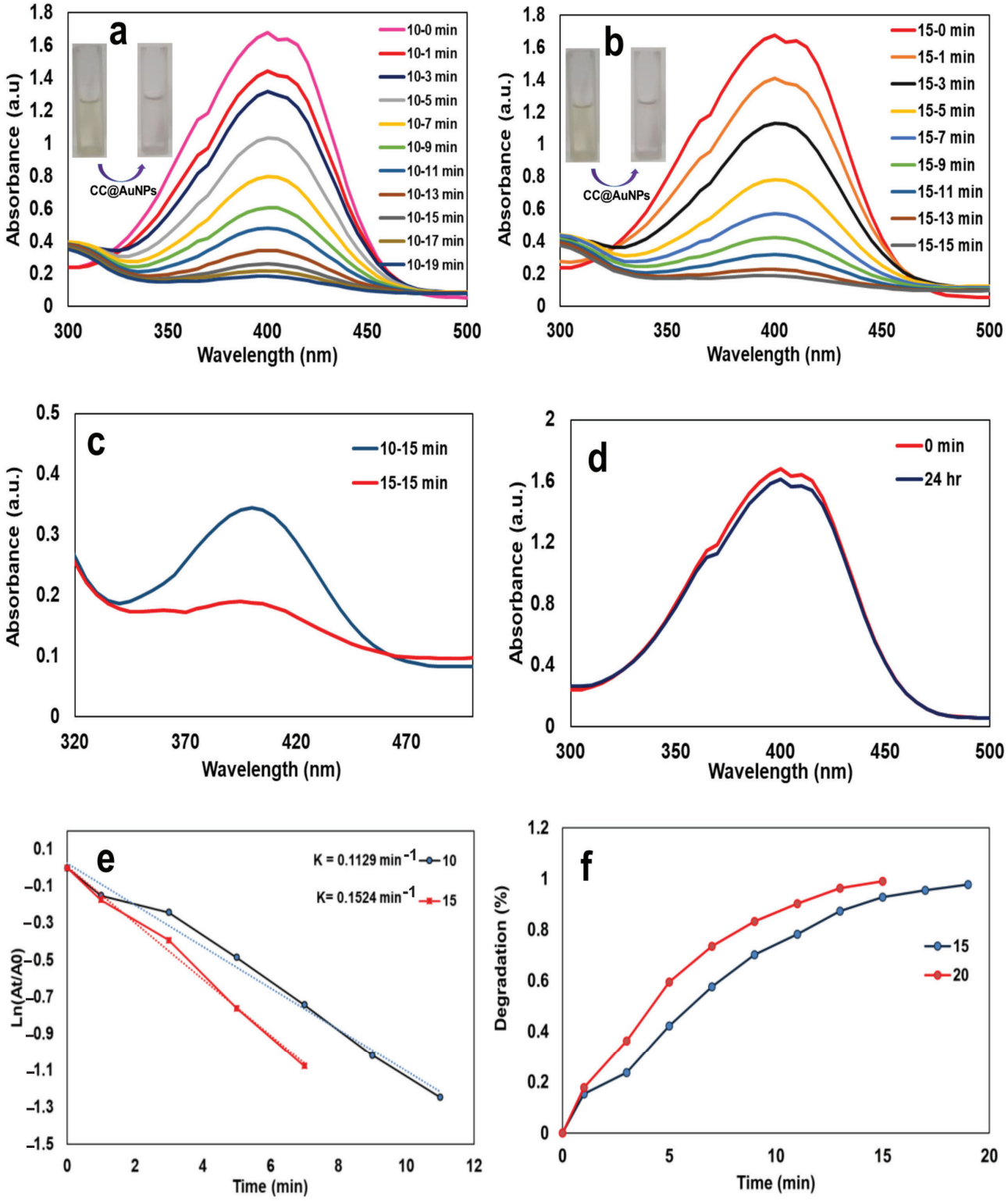


Figure 12. UV–Vis absorption spectra of 4-NP reduction with $NaBH_4$ catalyzed by (**a**) 10 µL, (**b**) 15 µL of CC-AuNPs (425 µg/mL), (**c**) the comparison of different volumes of CC-AuNPs (10 and 15 µL). (**d**) UV-Vis spectra of 4-NP reduction with $NaBH_4$ without nanocatalyst, (**e**) the corresponding plots of ln(At/A0) vs time, (**f**) degradation percentage of 4-NP.

In addition, the reduction of 4-NP by biosynthesized CC-AuNPs (10 and 15 µL) with NaBH4 was examined at 405 nm, changing from yellow to colorless with the removing the absorption peak at 405 nm over 19 and 15 min (Figure 12a–c). Figure 12d shows a com-

parison of the reduction times. Moreover, the degradation rate of 4-NP was pseudo-first order with a rate constant (K) of 0.1129 and 0.1524 min^{-1} (Figure 12e). Therefore, the rate constant improved using the addition of CC-AuNPs to the NaBH4 solution. The degradation percentages of 4-NP using 10 and 15 µL of the prepared CC-AuNPs were calculated 97.7 and 99%, respectively (Figure 12f). In addition, the results of the present study have been confirmed by previously published findings for green-synthesized AuNPs [72,73]. Therefore, the results indicated the excellent catalytic effect of biosynthesized CC-AuNPs in the degradation of three organic dyes of MO, MB, and 4-NP.

The catalytic potential of CC-AuNPs may be owing to their size; smaller AuNPs display higher surface area and simplify the adsorption of organic dye (MO/MB/4-NP) and BH_4^-. AuNPs operate as electron donors and acceptors and assist the electron transfer in a redox reaction, therefore transferring H^- to the surface of the dye (Figure 13) [69]. For 4-NP reduction by AuNPs, BH_4^- is adsorbed onto AuNPs as the catalytic surface, and the self-hydrolysis of BH_4^- produces BO_2^-. Temporarily, "the active surface-hydrogen" (Au-H) is formed when BH_4^- transfers "the active hydrogen species" to AuNPs. Afterward, 4-NP is reversibly attached to the Au surface. At the same time, "the active surface hydrogen" is transferred to -NO_2 and creates the corresponding amino group. Then, the desorption of produced aminophenol compounds from the catalyst surface was performed [74]. In addition, the AuNPs help the electron transfer from BH_4^- to MO and MB dyes, producing colorless compounds: leuko methyl orange and leuko methylene blue, respectively. It is assumed that the catalytic reduction of dyes is complete when the absorption intensity of MB and MO reach their baseline [75–77].

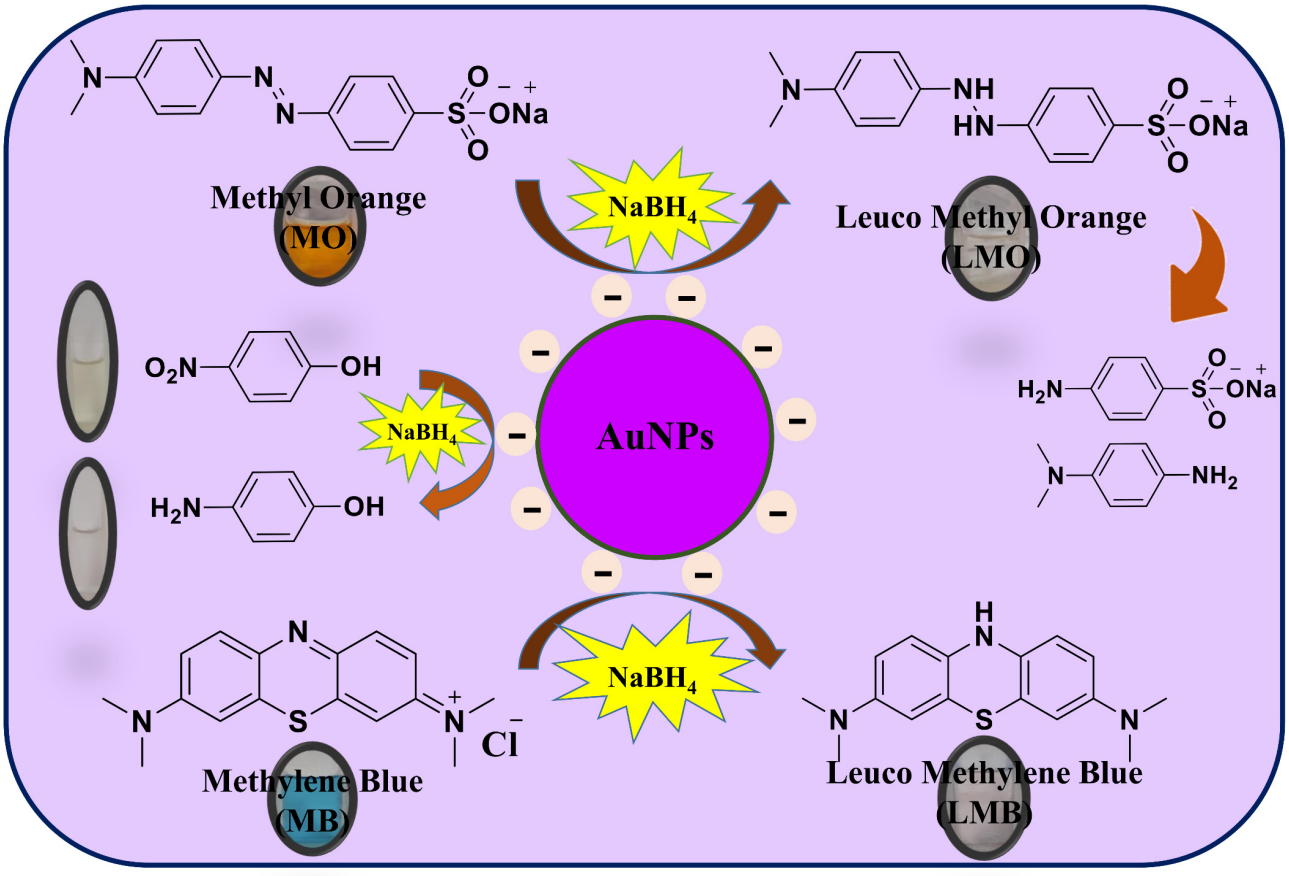


Figure 13. The mechanism of action of catalytic degradation of three dyes (MB, MO, and 4-NP) using biofabricated CC-AuNPs and $NaBH_4$ under visible light.

3. Materials and Methods

3.1. Materials

Chloroauric acid ($HAuCl_4 \cdot 3H_2O$) from Sigma Aldrich (St. Louis, MO, USA), 2,2-diphenyl-1-picrylhydrazyl from Merck (Schnelldorf, Germany), and sodium borohydride from Fluka were provided as analytical grade. In addition, methylene blue, methyl orange, and others were purchased from Merck India Ltd. Deionized water was used for all aqueous solutions.

3.2. Preparation of C. caspius Extract

The *C. caspius* was provided from the Mazandaran province of Iran. The whole plant was dried at room ambient for five days, and the dried plant was powdered using a blender. To prepare the plant extract, 20 g of the dried plant was extracted using methanol (90 mL) for 24 h through the maceration method at room temperature and then filtered through Whatman filter paper. To remove methanol, the filtrate was concentrated by a rotary evaporator and then freeze-dried. The obtained solid extract (about 4 g) was used during the synthesis of AuNPs.

3.3. Green Synthesis of C. caspius Extract-Mediated AuNPs

Different experimental conditions were tested for the green synthesis of *C. caspius* extract-mediated gold nanoparticles. The optimum condition was obtained through the investigation of $HAuCl_4 \cdot 3H_2O$ at different concentrations of 6.348 mM, 5.078 mM, 3.809 mM, 2.539 mM, and 1.269 mM in deionized water at 40, 60, 80, and 90 °C at 400 rpm. Then, 10 mL of the extract (25, 50, and 100 mg of the dried extract) was added to the reaction solution drop by drop. The yellow color of the mixture transformed to ruby red after about 30 min, demonstrating the reduction of the Au ions. UV–Vis spectrophotometer monitored the fabrication of the nanoparticles ranging from 200–800 nm. The produced gold nanoparticles were designated as CC-AuNPs, washed (with methanol and water successively), and then dried.

3.4. High-Pressure Liquid Chromatography (HPLC)

HPLC system comprised a model K-1001 solvent delivery system equipped with a Rheodyne injection valve (20 µL sample loop inserted) and a UV–Vis spectrophotometric detector (model K-2600) set at 285 nm. The analysis was conducted using an ODS (C18) column (250 mm × 4.6 mm, I.D., 5 mm particle size, Shim-pack VP-ODS). All solvents were degassed before injection.

A solution of acetonitrile, water, and formic acid (17:82.6:0.4) at 25 °C with a flow rate of 1 mL/min and a run period of 40 min was utilized as the mobile phase for separation. The detector was tuned to 280 nm to detect five standards at once. The purpose of this study was to determine the phytochemicals present in the plant by comparing the compounds' retention durations to authentic standards. Catechin, gallic acid, p-coumaric acid, caffeic acid, and rutin, all made by Sigma-Aldrich, were used as standards. The peak area of specific concentrations of the sample and standard was used to determine the amount of phenolic acids.

3.5. Characterization of the Synthesized Nanoparticles

The fabrication of AuNPs was checked by evaluating the absorbance of the mixture reaction on the UV–Vis spectrophotometer (T80 UV–Vis spectrophotometer PGI, Beijing, China) at 200–800 nm, when the solution color changed from yellow to ruby red color. Transmission electron microscopy (TEM) imaging (EM 208S, Philips, Eindhoven, Netherlands) was used to define the particle size and morphology. Field emission scanning electron microscope (FE-SEM) images were obtained using a TESCAN BRNO-Mira3 LMU (TESCAN, Brno, Czech Republic), and energy dispersive X-ray analysis (EDX) was applied along with FE-SEM to determine the elemental composition of synthesized nanoparticles. XRD patterns were recorded to determine the crystalline nature of the centrifuged and

dried CC-AuNPs using a x-rays diffractometer (X-PERT PRO, PANalytical, Almelo, The netherlands) (2θ = 10°–80°) with Cu Kα source (λ = 1.5406 A°). FT-IR spectra were recorded using an ATR FT-IR spectrometer (Cary 630, Agilent, Santa Clara, CA, USA) from 4000 to 650 cm^{-1}. The size distribution of the CC-AuNPs was determined by DLS analysis (dynamic light scattering). Thermogravimetric (TG) analysis and differential thermal analysis (DTA) was used to study the thermal properties of the CC-AuNPs in the range of 55–900 °C at a heating rate of 0.01–100 K/min on an autonomic TG/DTA (STA 503, BAHR, Hüllhorst, Germany).

3.6. Cytotoxic Activity of CC-AuNPs on MCF-7 and AGS Cells

MCF-7 cells (human breast cancer cell line), AGS cells (human gastric cancer cell line), and human embryonic kidney 293 cells (HEK cells) were cultured in RPMI-1640 and maintained with 10% fetal bovine serum (FBS) and 1% penicillin/streptomycin solution. Cultures were maintained at 37 °C, 5% CO_2 in a humid atmosphere [78].

Cell Maintenance and Culture Procedures

The MTT assay was used to determine cell viability. It is based on cellular dehydrogenases converting the dye MTT to formazan crystals, an insoluble intracellular product [79]. In addition, the cytotoxic effects of prepared nanoparticles on cellular proliferation was assessed by the MTT assay. AGS, MCF-7, and HEK cells were maintained at 37 °C, 5% CO_2 in a humidified incubator. The growth medium was removed after 24 h, and 100 µL of different concentrations of CC-AuNPs (1, 10, 25, 50, and 100 µg/mL) was added to the wells in triplicate with 10% FBS and antibiotics. Incubation was performed in the described conditions. Nontreated control cells (negative control) were also maintained to compare growth inhibition. After 24 h, the CC-AuNPs were removed from the wells, and 30 µL of MTT (3-(4,5-dimethylthiazol-2-yl)-2,5-diphenyltetrazolium bromide) solution (5 mg/mL in phosphate buffer saline (PBS)) was added to all wells (test and control) and incubated for 4 h. Then, the supernatant was removed from the wells and mixed with 100 µL of DMSO. Afterward, the 96 wells were incubated to solubilize formazan crystals (purple). The absorbance values of the mixture were measured using Synergy H1 hybrid multi-model microplate reader (Biotek Instruments, Winooski, Vermont, NE, USA) at 570 nm. The experiment was conducted in triplicate. Data produced were applied to plot a dose–response curve (log concentration vs response) using nonlinear regression with GraphPad Prism 8.0; the concentration of CC-AuNPs to kill 50% of cells was determined as the half-maximum inhibitory concentration (IC_{50}) [49]. The effect of the CC-AuNPs on cells proliferation was defined as the % cell viability, which was calculated by Equation (1) [5,49]:

$$\text{Cell viability (\%)} = (\text{Mean Asample}/\text{Acontrol}) \times 100 \quad (1)$$

3.7. Assaying the Minimum Inhibitory Concentration (MIC) and the Minimum Bactericidal Concentration (MBC) of CC-AuNPs

The antibacterial activity of the prepared CC-AuNPs against some American Type Culture Collection (ATCC) bacteria was investigated: *Enterococcus faecalis, Staphylococcus aureus* (gram-positive bacteria), *Proteus mirabilis*, *Klebsiella pneumoniae*, *Pseudomonas aeruginosa*, *Escherichia coli*, and *Acinetobacter baumannii* (gram-negative bacteria). The MIC value of CC-AuNPs was determined using the broth microdilution method in a 96-well microplate; 100 µL of Mueller–Hinton broth (MHB) medium was added to all wells, and then a serial dilution of the CC-AuNPs was transferred to each well of the microplate except one well. One hundred microliters of 0.5 McFarland turbidity standards from bacterial suspension was added to each of the 96 wells, and incubated at 37 °C for 24 h. The MIC is defined as the lowest concentration of the CC-AuNPs that entirely inhibits bacterial growth (no visible growth) [80]. To assess the minimum bactericidal concentration (MBC), 10 µL was sampled from the wells of 1 × MIC, 2 × MIC, 4 × MIC, and 8 × MIC, placed onto Mueller–Hinton agar plates, and incubated at 37 °C for 24 h. The MBC is determined as the lowest concentration of the CC-AuNPs that visibly inhibits bacterial growth on Mueller–Hinton

agar [81]. The positive and the negative control were studied as pure bacterial suspensions (without any NPs) and MHB (without any bacterial suspension), respectively. The reference antibiotic was ciprofloxacin.

3.8. Antileishmanial Activity

The effect of biosynthesized CC-AuNPs was investigated to Leishmania major promastigotes. In the process, several concentrations of CC-AuNPs, from 212.5 to 6.64 µg/mL, were used to evaluate the antileishmanial activity; 100 µL of CC-AuNPs was loaded to each well of a 96-well plate and serially diluted with RPMI-1640 medium. Then, 100 µL of medium with 1×10^5 promastigotes was added and incubated for 72 h at 24 °C. At that time, MTT solution (2.5 mg/5 mL PBS) was introduced to each well, and incubation was performed at 37 °C. Subsequently, the contents of each well were transferred to a microtube and centrifuged at 3000 rpm for 5 min, and the precipitate was dissolved in isopropyl alcohol. The absorbance of the 96-well plate was measured using the ELISA reader "Synergy H1 hybrid multi-model microplate reader (Biotek Instruments, Winooski, Vermont, NE, USA" at 492 nm. Three untreated wells containing the parasites were defined as negative controls. Amphotericin B was considered as the positive control. The experiment was performed in triplicate [82].

3.9. Antifungal Activity

The broth microdilution method was applied to determine MIC value based on "M27-A3 method from the Clinical and Laboratory Standards Institute (CLSI) formerly NCCLS". The tested strains included *Candida albicans* (IFRC1873), *Candida albicans* (IFRC1874), *Aspergillus fumigatus* (IFRC1649), *Aspergillus fumigatus* (IFRC1505), *Trichophyton mentagrophytes (FR1_22130)*, *Trichophyton mentagrophytes* (FR5_22130), *Fusarium proliferatum* (IFRC1871), and *Fusarium equiseti* (IFRC1872). Briefly, 100 µL of C@AuNPs was introduced to the microplate wells, then 100 µL of RPMI medium was added and serially diluted. After that, 100 µL of cell suspension was placed into each well. After 24 h (for *C. albicans*) and 48 h for other strains, visible growth was evaluated. Itraconazole was used as a reference antibiotic [83].

3.10. DPPH Free Radical Scavenging

The antioxidant potential of CC-AuNPs was measured by DPPH free radical scavenging assay; one milliliter of diphenyl-1-picrylhydrazyl solution (DPPH) that contained 2 mg of DPPH dissolved in 50 mL MeOH was spared to the CC-AuNPs (3.31 to 53 µg/mL), and incubated in the dark condition (15 min). Then, the absorbance values of the solution were recorded by UV–Vis spectrophotometer at 517 nm. Butylated hydroxyanisole (BHA) was the standard reference. All experiments were repeated three times. To calculate the inhibition percentage, Equation (2) was used:

$$\text{DPPH scavenging activity (\%)} = (\text{Ac} - \text{As/Ac}) \times 100 \quad (2)$$

Ac and As are defined as the absorbance value of the DPPH solution only and the absorbance of the CC-AuNPs solution, respectively. A linear regression method was applied to determine the IC_{50} value [5].

3.11. Catalytic Activity Assays

MO, MB, and 4-NP dyes were selected to assess the catalytic potential of synthesized CC-AuNPs in the presence of $NaBH_4$. In the process, 100, 120, and 150 µL of CC-AuNPs (425 µg/mL) was added to the solution, containing MO solution (50 µL × 5 mM), 2 mL H_2O, and NaBH4 (100 µL × 0.1 M) solution. For the MB degradation test, the various concentrations of CC-AuNPs (150, 170, and 200 µL) were mixed with the solution, including MB solution (30 µL × 10 mM), 5.77 mL H_2O, and $NaBH_4$ (200 µL × 0.1 M) solution. In the reduction of 4-nitrophenol (4-NP), prepared CC@AuNPs solution (10 and 15 µL) was mixed with a solution containing 4-NP solution (100 µL × 2 mM) and 2 mL H_2O mixed

with $NaBH_4$ solution (100 µL × 0.1 M). The absorption spectra of the reaction mixture were periodically determined using a UV–Vis spectrophotometer in the range of 200–800 nm. When the reduction reaction order was known to be pseudo-first order, the reaction kinetics were calculated using Equation (3):

$$\ln (At/A0) = -kt \quad (3)$$

where k is considered as a first-order rate constant (min^{-1}), t is defined as the reaction time, and A0 and At indicate the absorbance of the mixture before and after dye degradation, respectively.

3.12. Statistical Analysis

All the experiments were performed in triplicate. The GraphPad Prism 8.0 software performed a one-way analysis of variance (ANOVA) followed by Tukey's test; $p < 0.05$ was considered statistically significant.

4. Conclusions

Gold nanoparticles were successfully prepared using C. caspius extract as a cost-effective, eco-friendly, and accessible approach. The extract acts as a reducing and stabilizing agent in the preparation of gold nanoparticles from gold ions. The formation of AuNPs was confirmed by spectroscopic methods such as UV–Vis, DLS, EDX, TEM, FE-SEM, FT-IR, and XRD. The CC-extract-mediated AuNPs at optimum conditions of temperature, $HAuCl_4$, and extract concentration with a ruby red solution were formed at an SPR peak of 570 nm. The SEM and TEM images confirmed AuNPs with irregular shapes and an average size of around 22.66 ± 1.67 nm. The biosynthesized AuNPs indicated effective catalytic activity for degrading organic dyes and pollutants of MO, MB, and 4-NP. Based on the data obtained from biological investigations, the CC-AuNPs had potential antioxidant activity and exhibited moderate activity against several gram-positive and -negative bacteria. In addition, CC-AuNPs rarely showed antifungal effects against tested strains, while they displayed a higher antileishmanial effect than the positive control. They also showed excellent anticancer activity against AGS and MCF-7 cells with the IC_{50} concentrations at 48.2 µg/mL and 51.76 µg/mL, respectively. Therefore, our synthesized gold nanoparticles displayed various potential properties.

Author Contributions: Conceptualization, S.R.A. and M.A.E.; methodology, S.R.A. and P.B.; formal analysis, S.R.A. and B.A.K.; investigation, S.R.A.; Data curation, H.R.G.; resources, M.A.E.; funding, M.A.E.; writing—original draft, S.R.A., P.B., H.R.G., B.A.K. and M.A.E.; supervision, M.A.E.; writing—review and editing, M.A.E. All authors have read and agreed to the published version of the manuscript.

Funding: This research was supported by a grant from the Research Council of Mazandaran University of Medical Sciences, Iran (Grant No. 10555).

Data Availability Statement: The data will be available at the request of the corresponding author.

Conflicts of Interest: The authors declare that they have no competing interests.

References

1. Singh, A.K.; Tiwari, R.; Singh, V.K.; Singh, P.; Khadim, S.R.; Singh, U.; Laxmi; Srivastava, V.; Hasan, S.; Asthana, R. Green synthesis of gold nanoparticles from *Dunaliella salina*, its characterization and in vitro anticancer activity on breast cancer cell line. *J. Drug Deliv. Sci. Technol.* **2019**, *51*, 164–176. [CrossRef]
2. Wang, L.; Xu, J.; Yan, Y.; Liu, H.; Karunakaran, T.; Li, F. Green synthesis of gold nanoparticles from *Scutellaria barbata* and its anticancer activity in pancreatic cancer cell (PANC-1). *Artif. Cells Nanomed. Biotechnol.* **2019**, *47*, 1617–1627. [CrossRef] [PubMed]
3. Alizadeh, S.R.; Ebrahimzadeh, M.A. Characterization and anticancer activities of green synthesized CuO nanoparticles, A review. *Anti-Cancer Agents Med. Chem.* **2020**, *21*, 1529–1543. [CrossRef] [PubMed]
4. Ahmed, S.; Annu; Ikram, S.; Yudha, S. Biosynthesis of gold nanoparticles: A green approach. *J. Photochem. Photobiol. B Biol.* **2016**, *161*, 141–153. [CrossRef] [PubMed]

5. Hashemi, Z.; Mizwari, Z.M.; Mohammadi-Aghdam, S.; Mortazavi-Derazkola, S.; Ebrahimzadeh, M.A. Sustainable green synthesis of silver nanoparticles using *Sambucus ebulus* phenolic extract (AgNPs@ SEE): Optimization and assessment of photocatalytic degradation of methyl orange and their in vitro antibacterial and anticancer activity. *Arab. J. Chem.* **2022**, *15*, 103525. [CrossRef]
6. Suganya, K.U.; Govindaraju, K.; Kumar, V.G.; Dhas, T.S.; Karthick, V.; Singaravelu, G.; Elanchezhiyan, M. Blue green alga mediated synthesis of gold nanoparticles and its antibacterial efficacy against Gram positive organisms. *Mater. Sci. Eng. C* **2015**, *47*, 351–356. [CrossRef]
7. Soshnikova, V.; Kim, Y.J.; Singh, P.; Huo, Y.; Markus, J.; Ahn, S.; Castro-Aceituno, V.; Kang, J.; Chokkalingam, M.; Mathiyalagan, R.; et al. Cardamom fruits as a green resource for facile synthesis of gold and silver nanoparticles and their biological applications. *Artif. Cells Nanomed. Biotechnol.* **2018**, *46*, 108–117. [CrossRef]
8. Kumar, P.V.; Kala, S.M.J.; Prakash, K. Green synthesis of gold nanoparticles using *Croton caudatus* Geisel leaf extract and their biological studies. *Mater. Lett.* **2019**, *236*, 19–22. [CrossRef]
9. Shirzadi-Ahodashti, M.; Mortazavi-Derazkola, S.; Ebrahimzadeh, M.A. Biosynthesis of noble metal nanoparticles using crataegus monogyna leaf extract (CML@ X-NPs, X = Ag, Au): Antibacterial and cytotoxic activities against breast and gastric cancer cell lines. *Surf. Interfaces* **2020**, *21*, 100697. [CrossRef]
10. Ebrahimzadeh, M.A.; Naghizadeh, A.; Mohammadi-Aghdam, S.; Khojasteh, H.; Ghoreishi, S.M.; Mortazavi-Derazkola, S. Enhanced catalytic and antibacterial efficiency of biosynthesized Convolvulus fruticosus extract capped gold nanoparticles (CFE@ AuNPs). *J. Photochem. Photobiol. B Biol.* **2020**, *209*, 111949. [CrossRef]
11. Kajani, A.A.; Bordbar, A.-K.; Esfahani, S.H.Z.; Razmjou, A. Gold nanoparticles as potent anticancer agent: Green synthesis, characterization, and in vitro study. *RSC Adv.* **2016**, *6*, 63973–63983. [CrossRef]
12. Nagajyothi, P.; Lee, K.; Sreekanth, T. Biogenic synthesis of gold nanoparticles (quasi-spherical, triangle, and hexagonal) using Lonicera japonica flower extract and its antimicrobial activity. *Synth. React. Inorg. Met. Org. Chem.* **2014**, *44*, 1011–1018. [CrossRef]
13. Krishnaraj, C.; Muthukumaran, P.; Ramachandran, R.; Balakumaran, M.; Kalaichelvan, P. *Acalypha indica* Linn: Biogenic synthesis of silver and gold nanoparticles and their cytotoxic effects against MDA-MB-231, human breast cancer cells. *Biotechnol. Rep.* **2014**, *4*, 42–49. [CrossRef] [PubMed]
14. Nangia, Y.; Wangoo, N.; Goyal, N.; Shekhawat, G.; Suri, C.R. A novel bacterial isolate *Stenotrophomonas maltophilia* as living factory for synthesis of gold nanoparticles. *Microb. Cell Factories* **2009**, *8*, 39. [CrossRef]
15. Alhumaydhi, F.A.; Khan, I.; Rauf, A.; Qureshi, M.N.; Aljohani, A.S.; Khan, S.A.; Khalil, A.A.; El-Esawi, M.A.; Muhammad, N. Synthesis, characterization, biological activities, and catalytic applications of alcoholic extract of saffron (*Crocus sativus*) flower stigma-based gold nanoparticles. *Green Process. Synth.* **2021**, *10*, 230–245. [CrossRef]
16. Vijayakumar, R.; Devi, V.; Adavallan, K.; Saranya, D. Green synthesis and characterization of gold nanoparticles using extract of anti-tumor potent *Crocus sativus*. *Physica E Low Dimens. Syst. Nanostruct.* **2011**, *44*, 665–671. [CrossRef]
17. Abootorabi, Z.; Poorgholami, M.; Hanafi-Bojd, M.Y.; Hoshyar, R. Green synthesis of gold nanoparticles using Barberry and Saffron extracts. *Mod. Care J.* **2016**, *13*, e13000. [CrossRef]
18. Bogireddy, N.; Pal, U.; Gomez, L.M.; Agarwal, V. Size controlled green synthesis of gold nanoparticles using *Coffea arabica* seed extract and their catalytic performance in 4-nitrophenol reduction. *RSC Adv.* **2018**, *8*, 24819–24826. [CrossRef]
19. Sadeghi, B.; Mohammadzadeh, M.; Babakhani, B. Green synthesis of gold nanoparticles using *Stevia rebaudiana* leaf extracts: Characterization and their stability. *J. Photochem. Photobiol. B Biol.* **2015**, *148*, 101–106. [CrossRef]
20. Wu, Y.; Yang, Y.; Zhang, Z.; Wang, Z.; Zhao, Y.; Sun, L. A facile method to prepare size-tunable silver nanoparticles and its antibacterial mechanism. *Adv. Powder Technol.* **2018**, *29*, 407–415. [CrossRef]
21. Lee, K.; Nagajyothi, P.; Sreekanth, T.; Park, S. Eco-friendly synthesis of gold nanoparticles (AuNPs) using *Inonotus obliquus* and their antibacterial, antioxidant and cytotoxic activities. *J. Ind. Eng. Chem.* **2015**, *26*, 67–72. [CrossRef]
22. Vijayan, R.; Joseph, S.; Mathew, B. *Indigofera tinctoria* leaf extract mediated green synthesis of silver and gold nanoparticles and assessment of their anticancer, antimicrobial, antioxidant and catalytic properties. *Artif. Cells Nanomed. Biotechnol.* **2018**, *46*, 861–871. [CrossRef] [PubMed]
23. Asadi, M. Antioxidant and antimicrobial activities in the different extracts of Caspian saffron, *Crocus caspius* Fisch & CA Mey. ex Hohen. *Casp. J. Environ. Sci.* **2016**, *14*, 331–338.
24. Shokrzadeh, M.; Bakhshi Jouybari, H.; Talebpour Amiri, F.; Ziar, A.; Habibpour, P.; Habibi, E. Hepatoprotective activity of Caspian saffron (*Crocus caspius* Fisch and Mey) flowers against CCl4-induced acute liver injury in mice. *Res. J. Pharmacogn.* **2019**, *6*, 3339. [CrossRef]
25. Khalili, M.; Fathi, H.; Ebrahimzadeh, M.A. Antioxidant activity of bulbs and aerial parts of *Crocus caspius*, impact of extraction methods. *Pak. J. Pharm. Sci.* **2016**, *29*, 773–777. [PubMed]
26. Umamaheswari, C.; Lakshmanan, A.; Nagarajan, N. Green synthesis, characterization and catalytic degradation studies of gold nanoparticles against congo red and methyl orange. *J. Photochem. Photobiol. B Biol.* **2018**, *178*, 33–39. [CrossRef]
27. Liu, Y.; Huang, L.; Mahmud, S.; Liu, H. Gold nanoparticles biosynthesized using *Ginkgo biloba* leaf aqueous extract for the decolorization of azo-dyes and fluorescent detection of Cr(VI). *J. Clust. Sci.* **2020**, *31*, 549–560. [CrossRef]
28. Uzma, M.; Sunayana, N.; Raghavendra, V.B.; Madhu, C.S.; Shanmuganathan, R.; Brindhadevi, K. Biogenic synthesis of gold nanoparticles using *Commiphora wightii* and their cytotoxic effects on breast cancer cell line (MCF-7). *Process Biochem.* **2020**, *92*, 269–276. [CrossRef]

29. Khatua, A.; Priyadarshini, E.; Rajamani, P.; Patel, A.; Kumar, J.; Naik, A.; Saravanan, M.; Barabadi, H.; Prasad, A.; Paul, B.; et al. Phytosynthesis, characterization and fungicidal potential of emerging gold nanoparticles using *Pongamia pinnata* leave extract: A novel approach in nanoparticle synthesis. *J. Clust. Sci.* **2020**, *31*, 125–131. [CrossRef]
30. Balalakshmi, C.; Gopinath, K.; Govindarajan, M.; Lokesh, R.; Arumugam, A.; Alharbi, N.S.; Kadaikunnan, S.; Khaled, J.M.; Benelli, G. Green synthesis of gold nanoparticles using a cheap *Sphaeranthus indicus* extract: Impact on plant cells and the aquatic crustacean *Artemia nauplii*. *J. Photochem. Photobiol. B Biol.* **2017**, *173*, 598–605. [CrossRef]
31. Thangamani, N.; Bhuvaneshwari, N. Green synthesis of gold nanoparticles using Simarouba glauca leaf extract and their biological activity of micro-organism. *Chem. Phys. Lett.* **2019**, *732*, 136587. [CrossRef]
32. Sunderam, V.; Thiyagarajan, D.; Lawrence, A.V.; Mohammed, S.S.S.; Selvaraj, A. In-vitro antimicrobial and anticancer properties of green synthesized gold nanoparticles using *Anacardium occidentale* leaves extract. *Saudi J. Biol. Sci.* **2019**, *26*, 455–459. [CrossRef] [PubMed]
33. Srivastava, N.; Mukhopadhyay, M. Biosynthesis and characterization of gold nanoparticles using *Zooglea ramigera* and assessment of its antibacterial property. *J. Clust. Sci.* **2015**, *26*, 675–692. [CrossRef]
34. Anand, K.; Gengan, R.; Phulukdaree, A.; Chuturgoon, A. Agroforestry waste *Moringa oleifera* petals mediated green synthesis of gold nanoparticles and their anti-cancer and catalytic activity. *J. Ind. Eng. Chem.* **2015**, *21*, 1105–1111. [CrossRef]
35. Nasrollahzadeh, M.; Sajadi, S.M. Preparation of Au nanoparticles by *Anthemis xylopoda* flowers aqueous extract and their application for alkyne/aldehyde/amine A 3-type coupling reactions. *RSC Adv.* **2015**, *5*, 46240–46246. [CrossRef]
36. Hamelian, M.; Varmira, K.; Veisi, H. Green synthesis and characterizations of gold nanoparticles using *Thyme* and survey cytotoxic effect, antibacterial and antioxidant potential. *J. Photochem. Photobiol. B Biol.* **2018**, *184*, 71–79. [CrossRef]
37. El-Borady, O.M.; Ayat, M.S.; Shabrawy, M.A.; Millet, P. Green synthesis of gold nanoparticles using Parsley leaves extract and their applications as an alternative catalytic, antioxidant, anticancer, and antibacterial agents. *Adv. Powder Technol.* **2020**, *31*, 4390–4400. [CrossRef]
38. Li, S.; Shen, Y.; Xie, A.; Yu, X.; Qiu, L.; Zhang, L.; Zhang, Q. Green synthesis of silver nanoparticles using *Capsicum annuum* L. extract. *Green Chem.* **2007**, *9*, 852–858. [CrossRef]
39. Remya, R.; Rajasree, S.R.; Aranganathan, L.; Suman, T. An investigation on cytotoxic effect of bioactive AgNPs synthesized using *Cassia fistula* flower extract on breast cancer cell MCF-7. *Biotechnol. Rep.* **2015**, *8*, 110–115. [CrossRef]
40. Awwad, A.M.; Salem, N.M.; Abdeen, A.O. Noval approach for synthesis sulfur (S-NPs) nanoparticles using *Albizia julibrissin* fruits extract. *Adv. Mater. Lett.* **2015**, *6*, 432–435. [CrossRef]
41. Siregar, C.; Martono, S.; Rohman, A. Application of Fourier transform infrared (FTIR) spectroscopy coupled with multivariate calibration for quantitative analysis of curcuminoid in tablet dosage form. *J. Appl. Pharm. Sci.* **2018**, *8*, 151–156. [CrossRef]
42. Basavegowda, N.; Kumar, G.D.; Tyliszczak, B.; Wzorek, Z.; Sobczak-Kupiec, A. One-step synthesis of highly-biocompatible spherical gold nanoparticles using *Artocarpus heterophyllus* Lam.(jackfruit) fruit extract and its effect on pathogens. *Ann. Agric. Environ. Med.* **2015**, *22*, 84–89. [CrossRef] [PubMed]
43. Ravichandran, V.; Vasanthi, S.; Shalini, S.; Shah, S.A.A.; Tripathy, M.; Paliwal, N. Green synthesis, characterization, antibacterial, antioxidant and photocatalytic activity of Parkia speciosa leaves extract mediated silver nanoparticles. *Results Phys.* **2019**, *15*, 102565. [CrossRef]
44. Sun, Y.; Liu, W.; Tian, M.; Wang, L.; Wang, Z. A rational design of the sintering-resistant Au-CeO_2 nanoparticles catalysts for CO oxidation: The influence of H_2 pretreatments. *Materials* **2018**, *11*, 1952. [CrossRef]
45. Keshavamurthy, M.; Srinath, B.; Rai, V.R. Phytochemicals-mediated green synthesis of gold nanoparticles using *Pterocarpus santalinus* L. (Red Sanders) bark extract and their antimicrobial properties. *Part. Sci. Technol.* **2018**, *36*, 785–790. [CrossRef]
46. Sadiq, H.; Sher, F.; Sehar, S.; Lima, E.C.; Zhang, S.; Iqbal, H.M.; Zafar, F.; Nuhanović, M. Green synthesis of ZnO nanoparticles from *Syzygium cumini* leaves extract with robust photocatalysis applications. *J. Mol. Liq.* **2021**, *335*, 116567. [CrossRef]
47. Aljabali, A.A.; Akkam, Y.; Al Zoubi, M.S.; Al-Batayneh, K.M.; Al-Trad, B.; Abo Alrob, O.; Alkilany, A.M.; Benamara, M.; Evans, D.J. Synthesis of gold nanoparticles using leaf extract of *Ziziphus zizyphus* and their antimicrobial activity. *Nanomaterials* **2018**, *8*, 174. [CrossRef]
48. Padalia, H.; Chanda, S. Characterization, antifungal and cytotoxic evaluation of green synthesized zinc oxide nanoparticles using *Ziziphus nummularia* leaf extract. *Artif. Cells Nanomed. Biotechnol.* **2017**, *45*, 1751–1761. [CrossRef]
49. Lokina, S.; Narayanan, V. Antimicrobial and anticancer activity of gold nanoparticles synthesized from grapes fruit extract. *Chem. Sci. Trans.* **2013**, *2*, S105–S110. [CrossRef]
50. Taib, S.H.M.; Shameli, K.; Nia, P.M.; Etesami, M.; Miyake, M.; Ali, R.R.; Abouzari-Lotf, E.; Izadiyan, Z. Electrooxidation of nitrite based on green synthesis of gold nanoparticles using *Hibiscus sabdariffa* leaves. *J. Taiwan Inst. Chem. Eng.* **2019**, *95*, 616–626. [CrossRef]
51. Latif, M.; Abbas, S.; Kormin, F.; Mustafa, M. Green synthesis of plant-mediated metal nanoparticles: The role of polyphenols. *Asian J. Pharm. Clin. Res.* **2019**, *12*, 75–84. [CrossRef]
52. Ahmad, T.; Bustam, M.A.; Irfan, M.; Moniruzzaman, M.; Asghar, H.M.A.; Bhattacharjee, S. Mechanistic investigation of phytochemicals involved in green synthesis of gold nanoparticles using aqueous *Elaeis guineensis* leaves extract: Role of phenolic compounds and flavonoids. *Biotechnol. Appl. Biochem.* **2019**, *66*, 698–708. [CrossRef] [PubMed]
53. Choudhary, B.C.; Paul, D.; Gupta, T.; Tetgure, S.R.; Garole, V.J.; Borse, A.U.; Garole, D.J. Photocatalytic reduction of organic pollutant under visible light by green route synthesized gold nanoparticles. *J. Environ. Sci.* **2017**, *55*, 236–246. [CrossRef] [PubMed]

54. Bindhu, M.; Umadevi, M. Silver and gold nanoparticles for sensor and antibacterial applications. *Spectrochim. Acta Part A Mol. Biomol. Spectrosc.* **2014**, *128*, 37–45. [CrossRef]
55. Tao, C. Antimicrobial activity and toxicity of gold nanoparticles: Research progress, challenges and prospects. *Lett. Appl. Microbiol.* **2018**, *67*, 537–543. [CrossRef]
56. Ahmad, A.; Ullah, S.; Syed, F.; Tahir, K.; Khan, A.U.; Yuan, Q. Biogenic metal nanoparticles as a potential class of antileishmanial agents: Mechanisms and molecular targets. *Nanomedicine* **2020**, *15*, 809–828. [CrossRef]
57. Ahmad, A.; Syed, F.; Shah, A.; Khan, Z.; Tahir, K.; Khan, A.U.; Yuan, Q. Silver and gold nanoparticles from *Sargentodoxa cuneata*: Synthesis, characterization and antileishmanial activity. *RSC Adv.* **2015**, *5*, 73793–73806. [CrossRef]
58. Ahmad, A.; Syed, F.; Imran, M.; Khan, A.U.; Tahir, K.; Khan, Z.U.H.; Yuan, Q. Phytosynthesis and antileishmanial activity of gold nanoparticles by *Maytenus royleanus*. *J. Food Biochem.* **2016**, *40*, 420–427. [CrossRef]
59. El-Kassas, H.Y.; El-Sheekh, M.M. Cytotoxic activity of biosynthesized gold nanoparticles with an extract of the red seaweed *Corallina officinalis* on the MCF-7 human breast cancer cell line. *Asian Pac. J. Cancer Prev.* **2014**, *15*, 4311–4317. [CrossRef]
60. Priya, M.K.; Iyer, P.R. Anticancer studies of the synthesized gold nanoparticles against MCF 7 breast cancer cell lines. *Appl. Nanosci.* **2015**, *5*, 443–448. [CrossRef]
61. Eskandari-Nojedehi, M.; Jafarizadeh-Malmiri, H.; Rahbar-Shahrouzi, J. Hydrothermal green synthesis of gold nanoparticles using mushroom (*Agaricus bisporus*) extract: Physico-chemical characteristics and antifungal activity studies. *Green Process. Synth.* **2018**, *7*, 38–47. [CrossRef]
62. Khatoon, U.T.; Rao, G.N.; Mohan, M.K.; Ramanaviciene, A.; Ramanavicius, A. Comparative study of antifungal activity of silver and gold nanoparticles synthesized by facile chemical approach. *J. Environ. Chem. Eng.* **2018**, *6*, 5837–5844. [CrossRef]
63. Shabestarian, H.; Homayouni-Tabrizi, M.; Soltani, M.; Namvar, F.; Azizi, S.; Mohamad, R.; Shabestarian, H. Green synthesis of gold nanoparticles using sumac aqueous extract and their antioxidant activity. *Mater. Res.* **2016**, *20*, 264–270. [CrossRef]
64. Naraginti, S.; Li, Y. Preliminary investigation of catalytic, antioxidant, anticancer and bactericidal activity of green synthesized silver and gold nanoparticles using *Actinidia deliciosa*. *J. Photochem. Photobiol. B Biol.* **2017**, *170*, 225–234. [CrossRef] [PubMed]
65. Sathishkumar, G.; Jha, P.K.; Vignesh, V.; Rajkuberan, C.; Jeyaraj, M.; Selvakumar, M.; Jha, R.; Sivaramakrishnan, S. Cannonball fruit (*Couroupita guianensis*, Aubl.) extract mediated synthesis of gold nanoparticles and evaluation of its antioxidant activity. *J. Mol. Liq.* **2016**, *215*, 229–236. [CrossRef]
66. Pu, S.; Li, J.; Sun, L.; Zhong, L.; Ma, Q. An in vitro comparison of the antioxidant activities of chitosan and green synthesized gold nanoparticles. *Carbohydr. Polym.* **2019**, *211*, 161–172. [CrossRef]
67. Wang, L.; Lu, F.; Liu, Y.; Wu, Y.; Wu, Z. Photocatalytic degradation of organic dyes and antimicrobial activity of silver nanoparticles fast synthesized by flavonoids fraction of *Psidium guajava* L. leaves. *J. Mol. Liq.* **2018**, *263*, 187–192. [CrossRef]
68. Akilandaeaswari, B.; Muthu, K. Green method for synthesis and characterization of gold nanoparticles using *Lawsonia inermis* seed extract and their photocatalytic activity. *Mater. Lett.* **2020**, *277*, 128344. [CrossRef]
69. Nadaf, N.Y.; Kanase, S.S. Biosynthesis of gold nanoparticles by *Bacillus marisflavi* and its potential in catalytic dye degradation. *Arab. J. Chem.* **2019**, *12*, 4806–4814. [CrossRef]
70. León, E.R.; Rodríguez, E.L.; Beas, C.R.; Plascencia-Villa, G.; Palomares, R.A.I. Study of methylene blue degradation by gold nanoparticles synthesized within natural zeolites. *J. Nanomater.* **2016**, *2016*, 9541683. [CrossRef]
71. Suvith, V.; Philip, D. Catalytic degradation of methylene blue using biosynthesized gold and silver nanoparticles. *Spectrochim. Acta Part A Mol. Biomol. Spectrosc.* **2014**, *118*, 526–532. [CrossRef] [PubMed]
72. Shen, W.; Qu, Y.; Pei, X.; Li, S.; You, S.; Wang, J.; Zhang, Z.; Zhou, J. Catalytic reduction of 4-nitrophenol using gold nanoparticles biosynthesized by cell-free extracts of *Aspergillus* sp. WL-Au. *J. Hazard. Mater.* **2017**, *321*, 299–306. [CrossRef] [PubMed]
73. Sun, L.; Zhou, M.; Yin, Z.; Zhang, L.; Dou, B.; Su, W. Rapid synthesis of gold nanoparticles for photocatalytic reduction of 4-nitrophenol. *Res. Chem. Intermed.* **2020**, *46*, 5117–5131. [CrossRef]
74. Fu, Y.; Xu, P.; Huang, D.; Zeng, G.; Lai, C.; Qin, L.; Li, B.; He, J.; Yi, H.; Cheng, M.; et al. Au nanoparticles decorated on activated coke via a facile preparation for efficient catalytic reduction of nitrophenols and azo dyes. *Appl. Surf. Sci.* **2019**, *473*, 578–588. [CrossRef]
75. Irfan, M.; Moniruzzaman, M.; Ahmad, T.; Osman, O.Y.; Mandal, P.C.; Bhattacharjee, S.; Hussain, M. Stability, interparticle interactions and catalytic performance of gold nanoparticles synthesized through ionic liquid mediated oil palm leaves extract. *J. Environ. Chem. Eng.* **2018**, *6*, 5024–5031. [CrossRef]
76. Ganapuram, B.R.; Alle, M.; Dadigala, R.; Dasari, A.; Maragoni, V.; Guttena, V. Catalytic reduction of methylene blue and Congo red dyes using green synthesized gold nanoparticles capped by *Salmalia malabarica* gum. *Int. Nano Lett.* **2015**, *5*, 215–222. [CrossRef]
77. Velidandi, A.; Pabbathi, N.P.P.; Baadhe, R.R. Study of parameters affecting the degradation of rhodamine-B and methyl orange dyes by *Annona muricata* leaf extract synthesized nanoparticles as well as their recyclability. *J. Mol. Struct.* **2021**, *1236*, 130287. [CrossRef]
78. Devi, J.S.; Bhimba, B.V. Silver nanoparticles: Anti-bacterial and invitro cytotoxic activity. *IJBEES* **2012**, *2*, 2277–4394.
79. Mohseni Kouchesfehani, H.; Kiani, S.; Rostami, A.A.; Fakheri, R. Cytotoxic effect of iron oxide nanoparticles on mouse embryonic stem cells by MTT assay. *Iran. J. Toxicol.* **2013**, *7*, 849–853. Available online: http://ijt.arakmu.ac.ir/article-1-216-en.html (accessed on 4 February 2013).

80. Salari, Z.; Danafar, F.; Dabaghi, S.; Ataei, S.A. Sustainable synthesis of silver nanoparticles using macroalgae *Spirogyra varians* and analysis of their antibacterial activity. *J. Saudi Chem. Soc.* **2016**, *20*, 459–464. [CrossRef]
81. Chowdhury, N.R.; MacGregor-Ramiasa, M.; Zilm, P.; Majewski, P.; Vasilev, K. 'Chocolate' silver nanoparticles: Synthesis, antibacterial activity and cytotoxicity. *J. Colloid Interface Sci.* **2016**, *482*, 151–158. [CrossRef] [PubMed]
82. Ebrahimzadeh, M.A.; Hashemi, Z.; Mohammadyan, M.; Fakhar, M.; Mortazavi-Derazkola, S. In vitro cytotoxicity against human cancer cell lines (MCF-7 and AGS), antileishmanial and antibacterial activities of green synthesized silver nanoparticles using *Scrophularia striata* extract. *Surf. Interfaces* **2021**, *23*, 100963. [CrossRef]
83. Nidhin, M.; Saneha, D.; Hans, S.; Varghese, A.; Fatima, Z.; Hameed, S. Studies on the antifungal activity of biotemplated gold nanoparticles over Candida albicans. *Mater. Res. Bull.* **2019**, *119*, 110563. [CrossRef]

Disclaimer/Publisher's Note: The statements, opinions and data contained in all publications are solely those of the individual author(s) and contributor(s) and not of MDPI and/or the editor(s). MDPI and/or the editor(s) disclaim responsibility for any injury to people or property resulting from any ideas, methods, instructions or products referred to in the content.